Nature of the Boron–Phosphorus Bond in Monomeric Phosphinoboranes and Related Compounds

Doris C. Pestana and Philip P. Power*

Contribution from the Department of Chemistry, University of California, Davis, California 95616. *Received March 20, 1991*

Abstract: The nature of the bonding between boron and phosphorus in monomeric phosphinoboranes (also called borylphosphanes, i.e., $R_2BPR'_2$, R and R′ = hydrocarbyl groups, B and P three-coordinate) and related species has been studied in some detail. This was accomplished by the synthesis and detailed spectroscopic and structural characterization of a number of rare monomeric phosphinoboranes and related derivatives. These compounds are distinguished by the presence of B–P moieties in which there is a lone pair located on phosphorus adjacent to an empty boron p-orbital. The main conclusion of these studies is that there exist fundamental differences between the B–P compounds and their B–N analogues. The major reason for this is the presence of a large inversion barrier at the phosphorus center, rather than any inherent weakness in B–P π-bonds. The inversion barrier and the strength of the B–P π-interaction can be controlled by electronic and steric factors. In essence, increasing the size and the electropositive character of the phosphorus substituents increases the strength of the B–P π-bond. The compounds studied include $Mes_2BP(1\text{-Ad})H$, **1**; Mes_2BPPh_2, **2**; $Mes_2BP(t\text{-Bu})_2$, **3**; Mes_2BPMes_2, **4**; $Mes_2BP(1\text{-Ad})Li(Et_2O)_2$, **5**; $Mes_2BP(Ph)Li(Et_2O)$, **6**; $(Mes_2B)_2PPh$, **7**; $Mes_2BP(1\text{-Ad})PPh_2$, **8**; $Mes_2BP(Ph)SiPh_3$, **9**; and $Mes_2BP(1\text{-Ad})SiMe_3$, **10** (Mes = 2,4,6-$Me_3C_6H_2$, 1-Ad = 1-adamantanyl). They were examined by variable-temperature ^1H, ^{11}B, and ^{31}P NMR spectroscopy. Most compounds were also characterized by X-ray crystallography. The studies demonstrate that whereas the boron center is always planar, the phosphorus coordination can exhibit considerable geometrical variation between planarity and pyramidicity. There is a good correlation between the degree of pyramidicity at phosphorus and the B–P bond length, which can vary from 1.810 (4) Å for planar phosphorus to 1.948 (3) Å in the most pyramidal species. Variable-temperature ^1H NMR data for **1–3** and **10** reveal inversion barriers of <12.4, <10.4, and <9.7 kcal mol^{-1} for **1**, **2**, and **10**, whereas in the almost planar *tert*-butyl derivative **3** no dynamic behavior was obsereved as low as −97 °C. Rotational barriers of 12.4 and 16.9 kcal mol^{-1} were also found for **1** and **10**. The ^1H NMR data for the compounds **5–9**, which have essentially planar geometry at phosphorus, afford rotational barriers (kcal mol^{-1}) for the B–P multiple bond of 22.3 for **5**, 22.2 for **6**, 21.3 for **7**, 21.3 for **8**, and 17.1 for **9**. In summary, it may be concluded that B–P π-bonds are comparable in strength to B–N π-bonds. Crystal data with Mo Kα radiation (λ = 0.71069 Å) at 130 K: **1**, $C_{28}H_{38}BP$, monoclinic, $P2_1/c$, a = 9.461 (2) Å, b = 26.235 (10) Å, c = 10.415 (3) Å, β = 111.93 (2)°, R(3097$I > 3\sigma(I)$ data) = 0.050; **3**, $C_{26}H_{40}BP$, monoclinic $P2_1/c$, a = 23.530 (9) Å, b = 12.392 (5) Å, c = 18.119 (8) Å, β = 110.88 (3)°, R(3778$I > 3\sigma(I)$ data) = 0.077; **4**, $C_{36}H_{44}BP$, monoclinic, $P2/n$, a = 12.342 (4) Å, b = 7.703 (2) Å, c = 17.021 (5) Å, β = 108.94 (2)°, R(1973$I > 2\sigma(I)$ data) = 0.059; **5**, $C_{40}H_{67}O_3BPLi$, monoclinic, $P2_1/n$, a = 11.570 (2) Å, b = 20.203 (4) Å, c = 16.053 (5) Å, β = 95.84 (2)°, R(2595$I > 3\sigma(I)$ data) = 0.065; **9**, $C_{42}H_{42}BPSi$, triclinic, $P\bar{1}$, a = 9.112 (4) Å, b = 10.042 (6) Å, c = 19.479 (12) Å, α = 92.88 (5)°, β = 97.58 (5)°, γ = 97.03 (4)°, R(4180$I > 3\sigma(I)$ data) = 0.081; **10**, $C_{31}H_{46}BPSi$, orthorhombic, $P2_12_12_1$, a = 9.625 (5) Å, b = 11.067 (6) Å, c = 26.676 (12) Å, R(1958$I > 2\sigma(I)$ data) = 0.056.

Compounds that contain boron–phosphorus bonds have been known and studied for a long time. A common feature of the great majority of these is that both the boron and phosphorus centers are four coordinate.[1,2] Historically, lower coordination numbers (2 or 3) in B–P compounds have been much less numerous, and it is only within the past decade that the first examples were characterized by X-ray crystallography.[3] One of the simplest and most fundamental classes of the B–P compounds are the phosphinoboranes (or borylphosphanes), which may be represented by the simple formula $R_2BPR'_2$ (R or R′ = organic groups or a variety of other substituents that may include H, halogen, $-NR_2$, –OR, SR, etc.). A characteristic feature of phosphinoboranes is that they have a strong tendency to associate, in a head to tail manner, to give rings or oligomers having B–P frameworks with four-coordinate B and P centers as illustrated by the example of the cyclic trimer

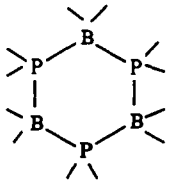

In this respect, they provide a sharp contrast to their B–N analogues the aminoboranes, $R_2BNR'_2$, which with a few exceptions, normally exist as monomers.[4,5] In addition, the aminoboranes, which are B–N analogues of the alkenes, possess a planar structure with a considerable rotation barrier around the B–N bond.[5] This is believed to be due to a π-interaction between the boron and nitrogen p-orbitals that, in effect, affords a B–N double bond. No such studies have appeared for the corresponding B–P compounds.

Early work on various phosphinoboranes suggested that monomers could exist. For example, cryoscopic data for low concentrations of species such as Ph_2BPPh_2, $(Ph_2B)_2PPh$, or $PhB(PPh_2)_2$ in benzene solution indicated a monomeric structure.[6] Bulkier analogues such as $Mes_2BP(C_6H_4\text{-}3\text{-}Me)_2$ or $(biphenyl)_2BP(C_6H_4\text{-}3\text{-}Me)_2$ were also isolated and characterized by IR spectroscopy.[6,7] In the light of presently available structural data (vide infra), there is no doubt that the former compound exists as a monomer in the solid. Molecular weight data for Me_2BPH_2 in ether[8] also indicated a monomeric formula, but polymerization occurred over a period of days.

Theoretical studies on the simplest B–P systems such as H_2BPH_2 have suggested that fundamental differences exist between phosphino- and aminoboranes.[9] This conclusion has been further

(1) Wasson, J. R. In *Gmelin Handbuch der Anorganischen Chemie. Erganzungswerk zur 8. Aufl. Bd. 19, Borverbindungen, Teil 3*; Springer: Berlin, 1975; p 93.
(2) Köster, R. In *Methoden der Organischen Chemie. Organobor-Verbindungen II: VI. Organobor-Phosphor -und -Arsen-Verbindungen*, Band XIII/3b; Georg Thieme Verlag: Stuttgart, 1983; p 386.
(3) For a review of phosphorus–boron compounds having B–P bonds with multiple character, see in the following reference: Power, P. P. *Angew. Chem., Int. Ed. Engl.* **1990**, *30*, 449.
(4) Niedenzu, K.; Dawson, J. W. *Boron-Nitrogen Compounds*; Springer-Verlag: Berlin, 1965.
(5) Lappert, M. F.; Power, P. P.; Sanger, A. R.; Srivastava, R. C. *Metal and Metalloid Amides*; Ellis-Horwood: Chichester, 1980.
(6) Coates, G. E.; Livingstone, J. G. *J. Chem. Soc.* **1961**, 5053.
(7) Coates, G. E.; Livingstone, J. G. *J. Chem. Soc.* **1961**, 1000.
(8) Burg, A. B.; Wagner, R. I. *J. Am. Chem. Soc.* **1953**, *75*, 3872. Burg, A. B. In *Advances in Boron and the Boranes*; Liebman, J. F., Greenberg, A., Williams, R. E., Eds.; VCH Verlagsgesellschaft, Weinheim, 1988; p 1.

0002-7863/91/1513-8426$02.50/0

supported by more recent calculations.[10,11] An important feature of these studies has been that the, apparently, low amount of π-donation from phosphorus lone pairs is not due to inherently weak first row– and second row orbital overlap but is due to the fact that planarization at phosphorus is very costly compared to the gain in π-resonance energy.[10c] Planar phosphine groups are comparable to amino groups in terms of their π-donor characteristics. It is the, often large, inversion barrier at phosphorus that significantly reduces the efficiency of such overlap.[10,11]

The main objective of the work described here is the experimental investigation of the factors that control the strength of B–P π-bonding. For this purpose, a variety of monomeric phosphinoboranes has been prepared, structurally characterized, and studied by variable-temperature ^{1}H, ^{11}B, and ^{31}P NMR spectroscopy. In addition, a range of other types of B–P compounds including boryldiphosphanes, lithium salts of borylphosphides, and diborylphosphanes have been studied. Together, the data show that a large variation in B–P multiple bonding is possible. Furthermore, this is largely determined by the steric and electronic properties of the substituents.

Experimental Section

General Procedures. All experiments were performed by using either modified Schlenk techniques or a Vacuum Atmosphere HE 43-2 drybox under N_2. Solvents were freshly distilled under N_2 from Na/K alloy–benzophenone ketyl and degassed three times immediately before use.

The reagents 1-AdP(O)Cl_2,[12] (*t*-Bu)$_2$PCl,[13] Mes_2PH,[14] and Mes_2BF[15] were prepared according to literature methods. $PhPCl_2$, Ph_2PCl, *n*-BuLi (1.6 M in hexane), and Ph_3SiCl were obtained commercially and used as received. 1-AdPH_2, (*t*-Bu)$_2$PH, $PhPH_2$, and Ph_2PH were prepared from their respective chlorides or oxychlorides by $LiAlH_4$ reduction. The synthesis of Mes_2BPPh_2, **2**, has been briefly described in a preliminary note;[16] further details are given here. The synthesis and structural characterization of $(Mes_2B)_2PPh$, **7**,[17] and Mes_2BP(1-Ad)PPh_2, **8**,[18] have also been reported previously. ^{31}P, ^{11}B, and ^{1}H NMR and variable-temperature ^{1}H NMR data were recorded on a QE-300 spectrometer operating at 121.70, 96.46, or 300.66 MHz, respectively. All ^{31}P spectra were referenced to external 85% H_3PO_4 and, with the exception of **1**, recorded with 2-W proton decoupling. The ^{11}B spectra were referenced to external BF_3·OEt_2. C_6D_6 was used as the solvent for room temperature spectroscopy. Variable-temperature studies were performed in C_7D_8, from room temperature to −99 °C and in *o*-C_8D_{10}, from −35 to +156 °C, in intervals of approximately 5 °C. IR spectra in the range of 4000–200 cm^{-1} were recorded on a Perkin-Elmer 1420 spectrometer by using Nujol mulls between CsI plates. Owing to the great number of bands in the expected B–P stretching range,[11] assignments of the B–P stretching frequency could not be made with certainty. The IR data collected for **1–3**, **5**, and **10** are provided in Table S8 of the supplementary material.

Mes_2BP(1-Ad)H (1). 1-AdPH_2 (1.62 g, 9.63 mmol) was dissolved in Et_2O (50 mL) and cooled in an ice bath. *n*-BuLi (6.1 mL of 1.6 M solution in hexane, 9.76 mmol) was added dropwise with stirring. The resulting pale yellow solution was then allowed to reach room temperature and was stirred for 1 h further. Mes_2BF (2.60 g, 9.69 mmol), dissolved in Et_2O (35 mL), was added dropwise through a cannula to the above solution at room temperature. The reaction was slightly exothermic, and yielded an orange solution and a white LiF precipitate. After 14 h of stirring, all the volatile compounds were pumped off and the orange residue was taken up in hexane (30 mL). The resulting solution was stirred for 2 h and then filtered and reduced in volume to incipient crystallization. Cooling at −16 °C for 3 days afforded yellow crystals suitable for X-ray structure determination. Yield: 1.37 g, 34.3%. Mp: 158–161 °C, softens at 145 °C. ^{1}H NMR (C_6D_6): δ = 1.48, 1.71, 1.99 (br s's, intensity ratio 2:1:2, 15 H, 1-Ad), 2.13 (s, 6 H, *p*-Me) 2.50 (s, 12 H, *o*-Me), 3.98 (d, 1 H, J_{P-H} = 275 Hz), 6.75 (s, 4 H, *m*-H). ^{11}B NMR (C_6D_6): δ = 83.8. ^{31}P NMR (C_6D_6): δ = 0.45 (d, J_{H-P} = 275 Hz). IR: ν(P–H) = 2330 and 2285 cm^{-1}.

Mes_2BPPh_2[16] (2). *n*-BuLi (1.6 M in hexane, 13.6 mL or 21.8 mmol) was added to a stirred solution of Ph_2PH (4.07 g, 21.8 mmol) in Et_2O (110 mL) with cooling in an ice bath. The intense yellow solution was allowed to reach room temperature and stirred for 2 h further. Mes_2BF (5.87 g, 21.9 mmol) dissolved in Et_2O (80 mL) was added dropwise through a cannula over a period of 45 min. The mixture became orange-yellow with deposition of a white precipitate. Stirring was continued for 10 h, and all volatile materials were then pumped off. The yellow residue was taken up in hexane (175 mL) and toluene (45 mL). Filtration, followed by volume reduction to ~40 mL under reduced pressure and cooling to −20 °C overnight, gave **2** as yellow crystals. Yield: 6.23 g, 65.6%. Mp: 119–123 °C. ^{1}H NMR (C_6D_6): δ, 2.02 (s, 6 H, *p*-Me), 2.28 (s, 12 H, *o*-Me), 6.60 (s, 4 H, *m*-H Mes), 6.82 (m, 6 H, *o,p*-H Ph), 7.17 (m, 4 H, *m*-H Ph). ^{31}P NMR (C_6D_6): δ = 26.7. ^{11}B NMR (C_6D_6): δ = 70.9.

$Mes_2BP(t\text{-}Bu)_2$ (3). (*t*-Bu)$_2$PH (3.17 g, 21.7 mmol) was dissolved in Et_2O (200 mL) at ~0 °C. *n*-BuLi (14 mL of a hexane 1.6 M solution, 22.4 mmol) was then added slowly. The resulting yellow mixture was allowed to come to room temperature and stirred for 1.5 h. It was then cooled again in an ice bath, and Mes_2BF (5.83 g, 21.7 mmol) was added slowly by a solid addition funnel. The orange-yellow mixture was allowed to warm to room temperature and stirred overnight. All the volatile material was pumped off, and the orange residue was taken up in hexane (30 mL). Filtration yielded a yellow solution, and upon reduction of volume to ~15 mL and cooling to −20 °C, an oily residue was obtained. The residue was dried for 2 h under reduced pressure and redissolved in pentane (25 mL). Filtration and volume reduction to ~8 mL and cooling in a −20 °C freezer produced yellow crystals adequate for an X-ray structure determination. Yield: 3.13 g, 36.6%. Mp: 102–105 °C (softens at 98 °C). ^{1}H NMR (C_7D_8): δ = 1.39 (d, 18 H, *t*-Bu, $^3J_{P-H}$ = 13.55 Hz), 2.31 (s, 6 H, *p*-Me), 2.74 (s, 12 H, *o*-Me), 6.90 (s, 4 H, *m*-H). ^{31}P NMR (C_7D_8): δ = 80.1. ^{11}B NMR (C_7D_8): δ = 61.9.

Mes_2BPMes_2 (4). *n*-BuLi (1.20 mL, 1.60 M, 1.92 mmol) was added by syringe to a stirred, ice-cooled solution of Mes_2PH (0.504 g, 1.86 mmol) in hexane (30 mL). The reaction mixture became pale yellow almost immediately. It was then stirred for 1 h at room temperature and warmed to its boiling point by use of a heat gun whereupon the yellow coloration greatly intensified. Stirring continued for a further 1 h. Mes_2BF (0.497 g, 1.85 mmol) dissolved in 35 mL of hexane was then added slowly to the solution by using a cannula and stirred overnight. The volume was reduced under reduced pressure to ~40 mL. Filtration followed by further volume reduction to ~8 mL and cooling in a −16 °C freezer overnight gave the product as very pale yellow, almost colorless crystals. Yield: 0.35 g, 36.3%. Mp: 147–150 °C. ^{31}P NMR (C_6D_6): δ = 27.4. ^{11}B NMR (C_6D_6): δ = 82.4. Crystals of **4** adequate for an X-ray structure determination were grown from an ether solution (5 mL).

Mes_2BP(1-Ad)Li(Et_2O) (5). *n*-BuLi (7.4 mL, 1.6 M, 11.8 mmol) was added slowly to an ether solution (45 mL) of AdPH_2 (1.98 g, 11.8 mmol) while cooling in an ice bath. The reaction mixture became yellow and eventually turbid when stirred for 2 h at room temperature. Mes_2BF (3.16 g, 11.8 mmol) dissolved in Et_2O (45 mL) was then added dropwise with cooling in an ice bath. The yellow coloration of the suspension became darker as the addition proceeded and the mixture was allowed to warm to room temperature and stirred for 8 h. With cooling in an ice bath, another 1 equiv of *n*-BuLi (7.4 mL, 1.6 M, 11.8 mmol) was added by syringe and the solution was stirred for a further 0.5 h. Stirring was continued for 2 h at room temperature, after which the pale orange solution was allowed to settle. Filtration through Celite followed by volume reduction to ca. 35 mL under reduced pressure and cooling overnight in a −20 °C freezer afforded the product as pale yellow, almost colorless, crystals that were suitable for X-ray structure determination. Yield: 3.62 g, 61.9% (only one Et_2O of solvation remained after drying under reduced pressure). Mp: 180–183 °C dec (it appears to desolvate further at 155 °C). ^{1}H NMR (C_6D_6): δ = 1.71 (br s, 6 H, CH_2 of 1-Ad), 1.91 (br s, 6 H, CH_2 of 1-Ad), 2.00 (br s, 3 H, bridgehead of 1-Ad), 2.19, 2.24 (2 s, 3 H each, *p*-Me), 2.52, 2.65 (2 s, 6 H each, *o*-Me), 6.86, 6.89 (2 s, 2 H each, *m*-H), 1.05 (t, 6 H, CH_3 of Et_2O), 3.30 (q, 4

(9) Gropen, O. *J. Mol. Struct.* **1977**, *36*, 111.
(10) (a) Magnusson, E. *Tetrahedron* **1985**, *41*, 5235; *Aust. J. Chem.* **1986**, *39*, 735. (b) Babon, J. A.; Roberts, B. P. *J. Chem. Soc., Perkin Trans. 2* **1987**, 487. (c) Schade, C.; von Ragué Schleyer, P. *J. Chem. Soc., Chem. Commun.* **1987**, 1399.
(11) (a) Allen, T. L.; Scheiner, A. C.; Schaefer, H. F., III. *Inorg. Chem.* **1990**, *29*, 1930. (b) We thank Professors T. L. Allen and W. H. Fink for the theoretical estimates of the energy and structural parameters for the orthogonal C_{2v} and C_s excited states of H_2BPH_2 and H_2BPH^-.
(12) Stetter, H.; Last, W. *Chem. Ber.* **1969**, *102*, 3364.
(13) Wold, A.; Ruff, J. K. *Inorg. Synth.* **1973**, *14*, 4.
(14) (a) Bartlett, R. A.; Olmstead, M. M.; Power, P. P.; Sigel, G. A. *Inorg. Chem.* **1987**, *26*, 1941. (b) Chen, H.; Olmstead, M. M.; Pestana, D. C.; Power, P. P. *Ibid.* **1991**, *30*, 1783.
(15) We thank Professor A. Pelter for a high-yield synthesis of Mes_2BF when the published procedure did not work in our hands. The method of synthesis is identical with that described for $(2,6\text{-}Me_2C_6H_3)_2BF$ in the following reference: Chen, H.; Bartlett, R. A.; Olmstead, M. M.; Shoner, S. C. *J. Am. Chem. Soc.* **1990**, *112*, 1048.
(16) Feng, X.; Olmstead, M. M.; Power, P. P. *Inorg. Chem.* **1986**, *25*, 4616.
(17) Bartlett, R. A.; Dias, H. V. R.; Power, P. P. *Inorg. Chem.* **1988**, *27*, 3919.
(18) (a) Pestana, D. C.; Power, P. P. *Inorg. Chem.* **1991**, *30*, 528; (b) *J. Am. Chem. Soc.* **1989**, *111*, 6887.

H, CH_2 of Et_2O). ^{31}P NMR (C_6D_6): δ = 90.4. ^{11}B NMR (C_6D_6): δ = 85.7.

$Mes_2BP(Ph)Li(Et_2O)$ (6). *n*-BuLi (7.90 mL, 1.6 M solution in hexane, 12.6 mmol) was added dropwise to an ice-cooled solution of $PhPH_2$ (1.39 g, 12.6 mmol) in Et_2O (25 mL) with rapid stirring. The resulting pale yellow suspension was stirred at ca. 0 °C for 10 min, allowed to reach room temperature, and then stirred for another 1.5 h before cooling again with an ice bath. Mes_2BF (3.39 g, 12.6 mmol) dissolved in Et_2O (35 mL) was added dropwise through a cannula to the previously cooled mixture over a period of 15 min. The addition was accompanied by a change in color from yellow to orange-yellow. Further stirring at room temperature for 5 h yielded a turbid orange solution, which was then cooled in an ice bath while a second 1 equiv of *n*-BuLi (7.9 mL, 1.6 M, 12.6 mmol) was added. The resulting amber mixture was stirred at 0 °C for 10 min and warmed to room temperature, whereupon stirring was continued for 2 h. The precipitate was allowed to settle after the volume had been reduced to ca. 15 mL. Filtration of the supernatant solution followed by extraction of the yellow residue with 4 × 15 mL of pentane gave a red solution. The product began to precipitate as a very fine crystalline yellow solid when the solution volume was reduced to ~50 mL. Further volume reduction to dryness afforded the crystalline product covered with a red oil, which was separated by washing with ~2 mL of hexane at ~0 °C and by removing the solution with a syringe. The product **6** was obtained as a crystalline dark yellow powder after drying the residue under reduced pressure for 20 min. Yield: 3.32 g, 60.1%. Mp: 139–142 °C (desolvates at 107 °C). ^1H NMR (C_6D_6): δ = 2.16, 2.22 (2 s, 3 H each, *p*-Me), 2.34, 2.60 (2 s, 6 H each, *o*-Me), 6.81, 6.84 (2 s, 2 H each, *m*-H), 6.97, 7.03 (2 m, 3 H, *p*- and *m*-H of Ph), 7.37 (d, 2 H, *o*-H of Ph), 0.83 (t, 6 H CH_3 of Et_2O), 3.04 (q, 4 H, CH_2 of Et_2O). ^{31}P NMR (C_6D_6): δ = 35.2. ^{11}B NMR (C_6D_6): δ = 58.4.

$(Mes_2B)_2PPh$ (7). The synthesis of this compound has been reported previously.[17] A modification of this procedure is described here. *n*-BuLi (3.95 mL, 1.6 M, 6.32 mmol) was added slowly to an ice-cooled solution of $PhPH_2$ (0.69 g, 6.3 mmol) in Et_2O (15 mL). The reaction mixture became yellow, and stirring was continued for 15 min at 0 °C, whereupon the solution was allowed to reach room temperature with continuous stirring for a further 1 h. The resulting yellow suspension was cooled in an ice bath, and Mes_2BF (1.68 g, 6.26 mmol) dissolved in Et_2O (18 mL) was added slowly by a double-tipped needle. The addition was accompanied by an intensification of the yellow color. After 3.5 h of stirring at room temperature, a further 1 equiv of *n*-BuLi (3.95 mL, 1.6 M, 6.32 mmol) was added with cooling in an ice bath. A second 1 equiv of Mes_2BF (1.68 g, 6.26 mmol), dissolved in 15 mL of Et_2O, was then added to the resulting orange-yellow suspension cooled in an ice bath. The orange coloration intensified as the addition proceeded. Stirring was continued for 2 h at ice temperature and then for 12 h at room temperature. The precipitate was allowed to settle, and the red supernatant solution was transferred by a double-tipped needle to another Schlenk tube. The yellow residue was washed with hexane, 3 × 25 mL. The combined washings and red solution were evaporated under reduced pressure to ~40 mL and then filtered by gravity through a glass frit. The bright orange-red filtrate was reduced in volume to incipient crystallization. The product was redissolved by heating in a 45 °C water bath. Cooling in a −15 °C freezer overnight afforded the product as small, yellow crystals. Yield: 1.08 g, 28.4%. Mp: 151–154 °C. ^1H NMR (C_8D_{10}, 60 °C): δ = 2.08, 2.12 (2 s, 6 H each, *p*-Me), 2.31, 2.48 (2 s, 12 H each, *o*-Me), 6.45, 6.55 (2 s, 4 H each, *m*-H), 6.94 (m, 5 H, Ph). ^{31}P NMR (C_8D_{10}): δ = 60.01. ^{11}B NMR (C_6D_6): δ = 47.8.

$Mes_2BP(1\text{-}Ad)PPh_2$ (8). This compound was prepared according to the procedure reported in the literature,[18a] and purified by recrystallization from ether. Yield: 41%. Mp: 167–170 °C. ^1H NMR (o-C_8D_{10}): δ = 1.51 (br m, 6 H, CH_2 of 1-Ad), 1.70 (br s, 3 H, bridgehead 1-Ad), 2.04, 2.07 (2 br s, 12 H, *p*-Me and CH_2 of 1-Ad), 2.38, 2.55 (2 s, 6 H each, *o*-Me), 6.40, 6.71 (2 s, 2 H each, *m*-H), 6.96, 7.63 (2 m, 10 H, Ph). ^{31}P NMR (C_6D_6): δ = −19.75, 19.55 (J_{P-P} = 316.5 Hz). ^{11}B NMR (C_6D_6): δ = 72.3.

$Mes_2BP(Ph)SiPh_3$ (9). *n*-BuLi (7.2 mL, 1.6 M solution in hexane, 11.5 mmol) was added dropwise by syringe to an ice-cooled ether solution (70 mL) of $PhPH_2$ (1.26 g, 11.4 mmol) with continuous stirring. The resulting pale yellow solution was stirred at 0 °C for 15 min and allowed to reach room temperature, whereupon stirring continued for 1 h. Mes_2BF (3.06 g, 11.4 mmol) dissolved in Et_2O (50 mL) was then added over a period of 0.5 h with cooling in an ice bath. The solution became bright yellow as the addition proceeded, and turbid after stirring for 5 h at room temperature. Another 1 equiv of *n*-BuLi (7.20 mL, 1.6 M, 11.5 mmol) was then added to the reaction mixture (maintained at 0 °C during addition) and stirred for 1 h at room temperature. The resulting orange-yellow suspension was cooled again in an ice bath while Ph_3SiCl (3.38 g, 11.4 mmol) dissolved in Et_2O (45 mL) was added slowly to it through a cannula. Turbidity disappeared during addition, and the yellow color became less intense. After 30 h of stirring, some very pale yellow crystals were observed on the glass wall above the surface of the solution. All volatiles were pumped off and the yellow residue taken up in hexane, 2 × 75 mL, and filtered through Celite to give a bright yellow solution that was then reduced in volume to ~8 mL. Cooling in a −15 °C freezer over 4 days gave the product as an oily precipitate. Recrystallization from ether (5 mL) afforded the product as very pale yellow, almost colorless, crystals that were suitable for an X-ray structure determination. Yield: 3.49 g, 49.6%. Mp: 161–163 °C. ^1H NMR (o-C_8D_{10}): δ = 2.22, 2.25 (2 s, 3 H each, *p*-Me), 2.49, 2.51 (2 s, 6 H each, *o*-Me), 6.47, 6.74 (2 s, 2 H each, *m*-H), 7.19 (mm, 14 H, *m*- and *p*-H of $SiPh_3$ and PhP), 7.82 (dd, 6 H, *o*-H of $SiPh_3$). ^{31}P NMR (o-C_8D_{10}): δ = −35.12. ^{11}B NMR (C_6D_6): δ = 72.0.

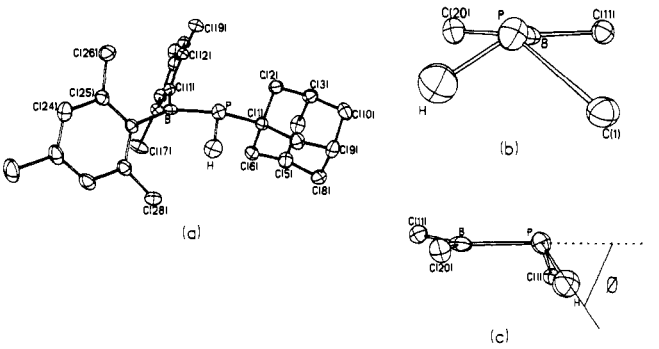

Figure 1. (a) Computer-generated thermal ellipsoid plot of **1**. Hydrogen atoms on carbon atoms are omitted for clarity. (b) View of the core atoms of **1** along the P–B bond axis. (c) View of the core atoms of **1** illustrating the out of plane angle at P.

$Mes_2BP(1\text{-}Ad)SiMe_3$ (10). $Mes_2BP(1\text{-}Ad)Li(Et_2O)_2$ was prepared in situ by treating an ice-cooled solution of $AdPH_2$ (0.94 g, 5.59 mmol) in Et_2O (20 mL) with *n*-BuLi (1.6 M, 3.5 mL, 5.60 mmol). After stirring for 1 h at room temperature, the yellow suspension was cooled in an ice bath and a solution of Mes_2BF (1.50 g, 5.59 mmol) in Et_2O (35 mL) was added dropwise. The resulting orange-yellow solution was allowed to reach room temperature and stirred for 3.5 h. A second 1 equiv of *n*-BuLi (1.6 M, 3.5 mL, 5.60 mmol) was then added with cooling in an ice bath. After stirring for 1 h at room temperature, an excess of Me_3SiCl (2.0 mL, 1.71 g, 15.8 mL) was added dropwise by syringe while the orange mixture was cooled in an ice bath. Within 5 min of the addition, the orange coloration disappeared and a white precipitate was observed. The resulting yellow suspension was stirred for 12 h, and the volatile materials were removed under reduced pressure. The yellow residue was taken up in pentane, 75 mL, and then filtered, and the volume was reduced to ~2 mL. Cooling in an acetone/dry ice bath overnight gave the product as yellow crystals, which were suitable for an X-ray structure determination. Yield: 2.53 g, 92.6%. Mp: 109–112 °C. ^1H NMR (C_6D_6): δ = 0.15 (d, 9 H, $SiMe_3$, $^3J_{P-H}$ = 5.2 Hz), 1.51 (br m, 6 H, CH_2 of 1-Ad), 1.72 (br m, 3 H, bridgehead 1-Ad), 2.04 (br m, 6 H, CH_2 of 1-Ad), 2.15 (s, 6 H, *p*-Me), 2.64 (2 s, 12 H, *o*-Me), 6.77, 6.80 (2 s, 4 H, *m*-H). ^{31}P NMR (C_6D_6): δ = 10.8. ^{11}B NMR (C_6D_6): δ = 66.2.

X-Ray Data Collection and the Solution and Refinement of the Structures. X-ray data for **1** and **3–5** were collected with a Syntex $P2_1$ diffractometer equipped with a graphite monochromator and a modified LT-1 low-temperature device. Crystallographic programs used were those of SHELXTL, Version 5, installed on a Data General Eclipse computer. A Siemens R3m/V diffractometer equipped with a graphite monochromator and a locally modified Enraf-Nonius LT apparatus was employed for data collection of **9** and **10**; calculations were carried out on a Micro VAX II computer using the SHELXTL program system. Neutral atom scattering factors and corrections for anomalous dispersion were from ref 19. Absorption corrections were made with the program XABS.[20] All compounds were coated with a layer of hydrocarbon oil upon removal from the Schlenk tube. A suitable crystal was selected, attached to a glass fiber by silicon grease, and immediately placed in the low-temperature N_2 stream.[21] Selected crystal data are provided in the abstract. Full details of the crystal data and refinement for **1**, **3–5**, **9**,

(19) *International Tables for X-Ray Crystallography*; Kynoch Press: Birmingham, England, 1974; Vol. IV.

(20) Hope, H.; Moezzi, B. *Program XABS*, University of California, Davis. This program obtains an absorption tensor from $F_o - F_c$ differences. Moezzi, B., Ph.D. Dissertation, University of California, Davis, 1987.

(21) This method is described in Hope, H. *ACS Symposium Series 357*; American Chemical Society: Washington, DC, 1987; Chapter 10.

Table I. Selected Structural Parameters for Compounds **1–5** and **7–10** and Other Related Compounds

	B–P, Å	$\Sigma°P$, deg[b]	ϕ,[c] deg	twist angle[d]	ref
TripB{PH(Mes)}{P(Mes)Li(Et_2O)$_2$} (**11**)[a]	1.810 (4)	359.4 (2)	7.8°	3.5°	30
	1.927 (3)	306.7 (13)	66.9°	9.6°	
Mes_2BP(1-Ad)Li(Et_2O)$_2$ (**5**)	1.823 (8)	357.4 (3)	16.1°	13.8°	this work
$Mes_2BP(SiMe_3)Li(THF)_3$ (**12**)	1.833 (6)	357.7 (2)	14.3°	23.15°	30
Mes_2BPMes_2 (**4**)	1.839 (8)	360.0 (3)	2.2°	2.8°	this work
$Mes_2BP(t\text{-}Bu)_2$ (**3**)	1.839 (8)	352.0 (3)	26.9°	14.5°	this work
	1.843 (8)	359.2 (3)	8.9°	21.8°	
$Mes_2BP(Ph)SiPh_3$ (**9**)	1.842 (6)	358.2 (2)	12.0°	10.4°	this work
Mes_2BP(1-Ad)$SiMe_3$ (**10**)	1.846 (8)	348.7 (3)	31.8°	16.7°	this work
Mes_2BPPh_2 (**2**)	1.859 (3)	339.4 (1)	42.1°	2.4°	16
Mes_2BP(1-Ad)PPh_2 (**8**)	1.858 (7)	350.0 (3)	27.5°	19.2°	18
$(Mes_2B)_2PPh$ (**7**)	1.871 (2)	360.0 (2)	0°	1.3°	17
Mes_2BP(1-Ad)H (**1**)	1.897 (3)	314.8 (12)	61.6°	7.5°	this work
tmp(Cl)BP(H)Mes (**13**)[e]	1.948 (3)	307.1 (10)	70°	~90°	29

[a] Trip = 2,4,6-*i*-$Pr_3C_6H_2$. [b] Sum of the angles at P bonded to boron. [c] Out-of-plane angle at P. [d] Defined as the angle between the perpendiculars to the B and P planes when viewed down the P–B bond axis. [e] tmp = 2,2,6,6-tetramethylpiperidine.

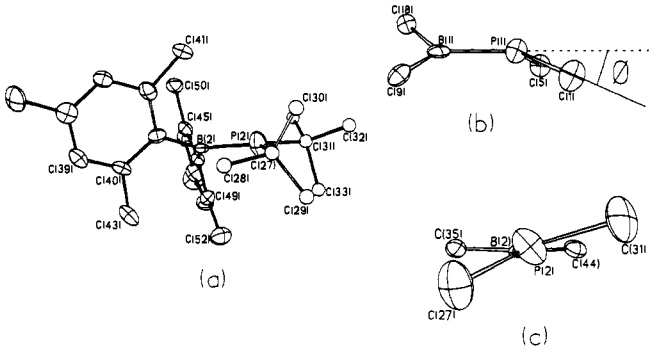

Figure 2. (a) Computer-generated thermal ellipsoid of **3**. Hydrogen atoms are omitted, and C(27)–C(34) are plotted as open circles for clarity. (b) View of the core atoms of **3** illustrating the out of plane angle at P(1). (c) View of the core atoms of **3** along the P(2)–B(2) bond axis.

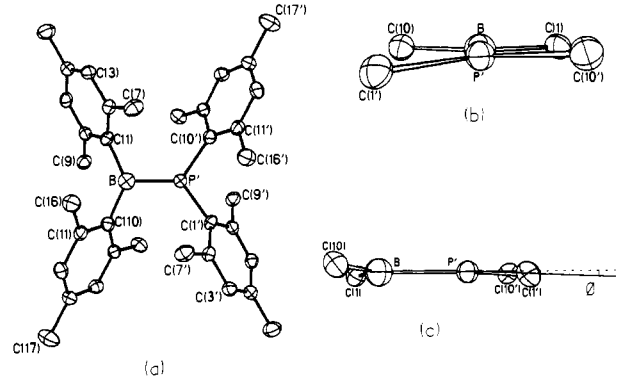

Figure 3. (a) Computer-generated thermal ellipsoid plot of **4**. Hydrogen atoms are omitted for clarity. (b) View of the core atoms of **4** along the P′–B bond axis. (c) View of the core atoms of **4** illustrating the out of plane angle at P′.

and **10** are described in Table S1 of the supplementary material. Notes on the solution of each structure are also provided therein.

Results

Structural Descriptions. The structures of **1**, **3–5**, **9**, and **10** are described here. The structures of the compounds **2**,[16] **7**,[17] and **8**[18] have already been reported. Important structural details for all compounds are summarized in Table I.

Mes_2BP(1-Ad)H (1). The molecular structure of **1**, which is illustrated in Figure 1a, consists of well-separated molecules of Mes_2BP(1-Ad)H that have no symmetry restrictions. A view down the P–B bond, which is 1.897 (3) Å long, is presented in Figure 1b. The angle between the planes containing the bisectors of H–P–C(1) and C(11)–B–C(20) angles is 7.5°. The P atom has pyramidal coordination, with an out of plane angle (ϕ) at P (Figure 1c) of 61.6°. The sum of the angles at P is 314.8°. The P–C(1) and P–H bond lengths are 1.871 (3) and 1.35 (3) Å, respectively. The boron center is planar with angles that deviate as much as 6.1° from regular trigonal values. The B–C(11) and B–C(20) bonds are 1.580 (3) and 1.578 (4) Å. The angles between the boron plane and the C(11) and C(20) mesityl rings are 60.4 and 68.2°, respectively.

$Mes_2BP(t\text{-}Bu)_2$ (3). The structure of **3**, illustrated in Figure 2a, consists of well-separated molecules of $Mes_2BP(t\text{-}Bu)_2$. The asymmetric unit contains two chemically identical, but crystallographically independent, molecules that have similar structures. The phosphorus atoms show some deviation from planarity in each molecule. However, the sum of the angles at P(1) and at P(2), which are 352.0° and 359.2°, are somewhat different. Thus, the out of plane angle at P(1) (26.9°) is larger than the one observed at P(2), which is 8.9° (Figure 2b). The different pyramidicities at P(1) and P(2) are reflected in slightly different P(1)–B and P(2)–B bond lengths of 1.839 (8) and 1.843 (8) Å; the average P–B bond length is thus 1.841 (8) Å. The molecules also differ in respect of the angles (14.5° and 21.8°) between the planes containing the bisectors of the C–P–C and C–B–C angles (Figure 2c). The P–C bond lengths vary from 1.851 (9) to 1.874 (7) Å. The boron centers are planar, with angles at boron that are close (within 2.0°) to the idealized angle of 120°. The average angle between the boron planes and the mesityl rings is 64.1°.

Mes_2BPMes_2 (4). The molecular structure of **4** is illustrated in Figure 3a. It consists of discrete units of Mes_2BPMes_2 with no short intermolecular contacts. The boron and phosphorus atoms are statistically disordered in their positions with respect to a 2-fold axis perpendicular to the B–P bond. The B–P separation at each site is 0.379 (8) Å, and the B–P′ bond is 1.839 (8) Å long. A view down the B–P′ bond, Figure 3b, shows an angle of 2.8° between the planes containing the bisectors of the angles C(1′)–P′–C(10′) and C(1)–B–C(10). The phosphorus atom has planar coordination, with irregular angles in the range of 109.9–125.4° and an out of plane angle at P of only 2.2°. The P atom deviates 0.03 Å from the C(1′)C(10′)B plane. The P–C(1′) and P–C(10′) bonds are 1.789 (3) and 1.801 (4) Å. The boron center is planar, and the B–C(1) and B–C(10) bond lengths are 1.611 (8) and 1.606 (10) Å, respectively. The angles between the boron plane and the C(1) and C(10) mesityl rings are 63.4 and 58.0°, respectively.

Mes_2BP(1-Ad)Li(Et_2O)$_2$ (5). The molecular structure of **5** is illustrated in Figure 4a and consists of well-separated molecules of Mes_2BP(1-Ad)Li(Et_2O)$_2$ that have no imposed crystallographic symmetry. A view down the P–B bond (Figure 4b), which has a length of 1.823 (8) Å, illustrates the angle of 13.8° between the planes containing the bisectors of the angles Li–P–C(1) and C(11)–B–C(20). The coordination at phosphorus approaches planarity, and the sum of the angles at P is 357.4° with an out of plane angle at P of 16.1° (Figure 4c). The P–C(1) and P–Li bond lengths are 1.882 (6) and 2.44 (1) Å, and the Li–O(1) and Li–O(2) bonds are 1.95 (1) and 1.92 (1) Å long. The angles at Li show minor deviations (<4°) from the regular trigonal values. The boron coordination is planar, with irregular angles in the range of 111.5–130.5°. The B–C(11) and B–C(20) bonds are 1.599

Table II. ^{11}B, ^{31}P, and Selected ^1H NMR Data at Room Temperature in C_6D_6 for Compounds **1–10**

compound	^{11}B	^{31}P	^1H (mesityl signals)		
			p-Me	*o*-Me	*m*-H
$Mes_2BP(1\text{-}Ad)H$ (**1**)	83.8	0.45 J_{P-H} = 275 Hz	2.13 (s, 6 H)	2.50 (s, 12 H)	6.75 (s, 4 H)
Mes_2BPPh_2 (**2**)	70.9	26.7	2.02 (s, 6 H)	2.28 (s, 12 H)	6.60 (s, 4 H)
$Mes_2BP(t\text{-}Bu)_2$ (**3**)[a]	61.9	80.1 $^3J_{P-H}$ = 13.6 Hz	2.31 (s, 6 H)	2.74 (s, 12 H)	6.90 (s, 4 H)
Mes_2BPMes_2 (**4**)	82.4	27.4			
$Mes_2BP(1\text{-}Ad)Li(Et_2O)_2{\cdot}Et_2O$ (**5**)	85.7	90.4	2.19 (s, 3 H) 2.24 (s, 3 H)	2.52 (s, 6 H) 2.65 (s, 6 H)	6.86 (s, 2 H) 6.89 (s, 2 H)
$Mes_2BP(Ph)Li(Et_2O)$ (**6**)	58.4	35.2	2.16 (s, 3 H) 2.22 (s, 3 H)	2.34 (s, 6 H) 2.60 (s, 6 H)	6.81 (s, 2 H) 6.84 (s, 2 H)
$(Mes_2B)_2PPh$ (**7**)[b]	47.8	60.1	2.08 (s, 6 H) 2.12 (s, 6 H)	2.31 (s, 12 H) 2.48 (s, 12 H)	6.45 (s, 4 H) 6.55 (s, 4 H)
$Mes_2BP(1\text{-}Ad)PPh_2$ (**8**)	72.3	−19.75, 19.55 J_{P-P} = 316.5 Hz	2.03 (s, 3 H) 2.06 (s, 9 H)[c]	2.45 (s, 6 H) 2.60 (s, 6 H)	6.47 (s, 2 H) 6.76 (s, 2 H)
$Mes_2BP(Ph)SiPh_3$ (**9**)[d]	72.0	−35.1	2.22 (s, 3 H) 2.25 (s, 3 H)	2.49 (s, 6 H) 2.51 (s, 6 H)	6.47 (s, 2 H) 6.74 (s, 2 H)
$Mes_2BP(1\text{-}Ad)SiMe_3$ (**10**)	66.2	10.8 $^3J_{P-H}$ = 5.2 Hz	2.15 (s, 6 H)	2.64 (d, 12 H)	6.77 (s, 2 H) 6.80 (s, 2 H)

[a] In C_7D_8. [b] ^1H NMR data in *o*-C_8D_{10}. [c] 6 H for CH_2 of the 1-Ad group. [d] ^1H and ^{31}P NMR in *o*-C_8D_{10}.

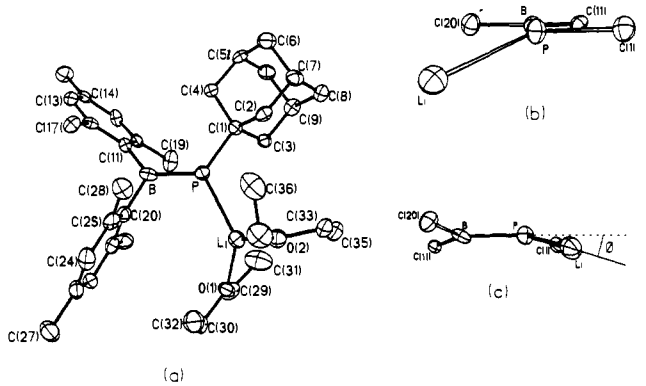

Figure 4. (a) Computer-generated thermal ellipsoid plot of **5**. Hydrogen atoms are omitted for clarity. (b) View of the core atoms of **5** along the P–B bond axis. (c) View of the core atoms of **5** illustrating the out of plane angle at P.

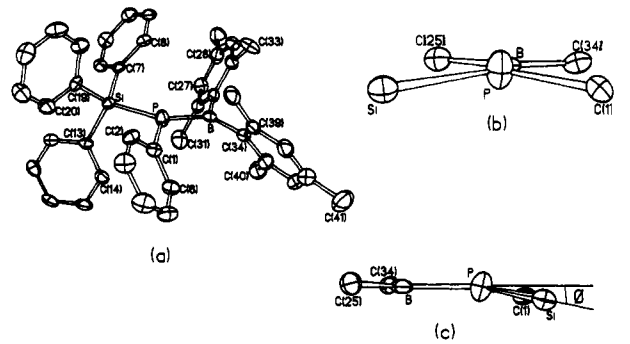

Figure 5. (a) Computer-generated thermal ellipsoid plot of **9**. Hydrogen atoms are omitted for clarity. (b) View of the core atoms of **9** along the P–B bond axis. (c) View of the core atoms of **9** illustrating the out of plane angle at P.

(9) and 1.605 (9) Å long. The angles between the boron plane and the C(11) and C(20) mesityl rings are 63.2 and 68.4°, respectively.

$Mes_2BP(Ph)SiPh_3$ (9). The structure of **9** is illustrated in Figure 5a. It consists of well-separated molecules of $Mes_2BP(Ph)SiPh_3$ that have no imposed symmetry restrictions. A view along the P–B bond, which is 1.842 (6) Å, is presented in Figure 5b. The angle between the planes containing the bisectors of the Si–P–C(1) and C(25)–B–C(34) angles is 10.4°. The coordination of the phosphorus center approaches planarity, with an out of plane angle at P of 12.0°, (Figure 5c). The P atom deviates 0.15 Å from the SiC(1)B plane. The sum of the angles at P is 358.2°, and their values are in the range of 110.3–131.2°. The boron center is planar, with angles that are within 4.4° of the idealized trigonal value. The B–C(25) and B–C(34) bond lengths are 1.590 (8) and 1.585 (7) Å, and the torsional angles between the boron plane and the C(25) and C(34) mesityl rings are 67.3 and 55.0°, respectively. The P–C(1) and P–Si bonds are 1.815 (5) and 2.231 (2) Å long. The Si–C bonds average 1.875 (8) Å. The angles at Si present deviations of less than 5° from regular tetrahedral values.

$Mes_2BP(1\text{-}Ad)SiMe_3$ (10). The structure of **10** is illustrated in Figure 6a. It involves well-separated units of $Mes_2BP(1\text{-}Ad)SiMe_3$ that have no imposed crystallographic symmetry. A view down the P–B bond, which is 1.846 (8) Å long, is illustrated in Figure 6b. It can be seen that the P–C(4) bond is almost exactly aligned with the C(14)BC(23) plane (torsional angle C(4)–P–B–C(14) = 5.8°), whereas the P–Si bond shows a fairly large angular deviation (torsional angle Si–P–B–C(23) = 39.0°). The angle between the planes containing the bisectors of Si–P–C(4)

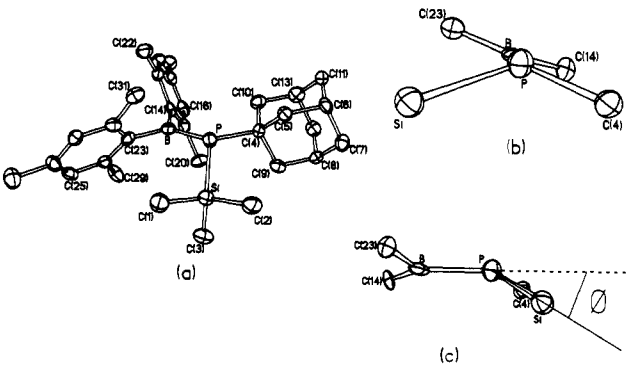

Figure 6. (a) Computer-generated thermal ellipsoid plot of **10**. Hydrogen atoms are omitted for clarity. (b) View of the core atoms of **10** along the P–B bond axis. (c) View of the core atoms of **10** illustrating the out of plane angle at P.

and C(23)–B–C(14) angles is 16.7°. The deviation of the phosphorus center from planarity is reflected in an out of plane angle at P of 31.8° (Figure 6c) and the sum of the angles at P of 348.7°. The B–C(14) and B–C(23) bond lengths are 1.576 (10) and 1.596 (10) Å, and the angles between the boron plane and C(14) and C(23) mesityl rings are 70.0 and 58.3°. The P–C(4) and P–Si bonds are 1.873 (6) and 2.263 (3) Å long, and the Si–C bonds average 1.856 (7) Å.

^{11}B, ^{31}P, and Variable-Temperature ^1H NMR Studies. Table II presents, in addition to the ^{11}B and ^{31}P NMR data, selected ^1H NMR chemical shifts and peak assignments for compounds **1–10** (in C_6D_6) at room temperature. The dynamic behavior of compounds **1–3** and **5–10** in solution was studied by monitoring

Table III. Variable-Temperature ^{1}H NMR and ΔG^* Data for Compounds **1–3** and **5–10**

compound	$\Delta\nu$, Hz			T_c, K			ΔG^*_{rot} kcal mol^{-1}			ΔG^*_{inv}, kcal mol^{-1}		
	p-Me	*o*-Me	*m*-H	*p*-Me	*o*-Me	*m*-H	*p*-Me	*o*-Me	*m*-H	*p*-Me	*o*-Me	*m*-H
$Mes_2BP(1\text{-}Ad)H$ (**1**)	22.7	103.3[a]	52.1[a]	247	259	254	12.4	12.3	12.4	>12.4	>12.3	>12.4
Mes_2BPPh_2 (**2**)		>10.1	>11.7[b]		201	<175					<10.4	<8.9
$Mes_2BP(t\text{-}Bu)_2$ (**3**)[b]		>24.0	>10.2		<176	<176					<8.7	<9.0
$Mes_2BP(1\text{-}Ad)Li(Et_2O)_2$ (**5**)	5.41	54.1	15.0	411	>425 (450)[c]	>425 (428)[c]	22.3	>21.1	>22.2			
$Mes_2BP(Ph)Li(Et_2O)$ (**6**)	14.9	104.1	41.0	424	>424 (458)[c]	>424 (438)[c]	22.2	>20.5	>21.3			
$(Mes_2B)_2PPh$ (**7**)	12.3	52.62	34.6	403	>425 (428)[c]	423	21.2	>21.2	21.4			
$Mes_2BP(1\text{-}Ad)PPh_2$ (**8**)	6.86	50.9	93.4	393	429	>429 (439)[d]	21.1	21.4	>20.9			
$Mes_2BP(Ph)SiPh_3$ (**9**)	9.92	7.22	86.3	323	320	359	17.0	17.0	17.4			
$Mes_2BP(1\text{-}Ad)SiMe_3$ (**10**)	3.91	5.71	8.12	275	316		14.9	16.9	?			
	12.9	47.5[e]	17.1[e]		199	184					<9.7	<9.3

[a] $\Delta\nu$ taken as the average of the differences in frequencies between the three singlets at lowest T measured. [b] Minimum $\Delta\nu$ is taken as $\nu_{1/2}$ of broad signal at lowest T measured. [c] Value extrapolated by using the rotation barrier calculated with the *p*-Me data [d] Value extrapolated by using the rotation barrier calculated with the *o*-Me data. [e] Minimum $\Delta\nu$ is taken as half of $\nu_{1/2}$ of broad signal at lowest T measured.

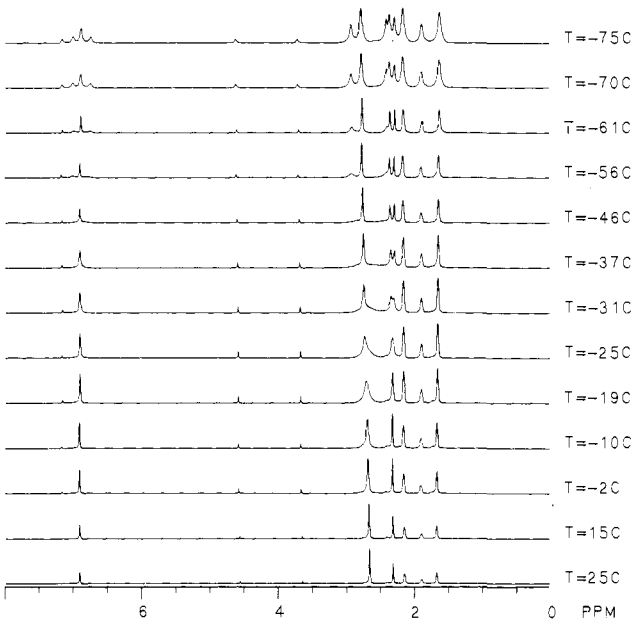

Figure 7. Stacked plot of the variable-temperature ^{1}H NMR spectra of **1** in C_7D_8.

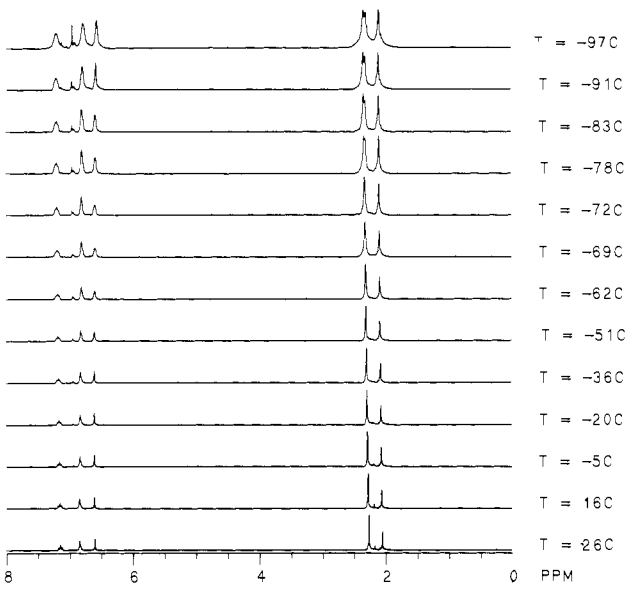

Figure 8. Stacked plot of the variable-temperature ^{1}H NMR spectra of **2** in C_7D_8.

the splitting of the *o*-Me, *p*-Me, and *m*-H signals of the boron mesityl groups. Rotational and inversion barriers were calculated by using an approximate formula as previously described.[22] Table III summarizes the variable-temperature ^{1}H NMR data collected for compounds **1–3** and **5–10**.

$Mes_2BP(1\text{-}Ad)H$ (1). The VT ^{1}H NMR spectrum of **1** is illustrated in Figure 7. At $T > 15$ °C, the *o*-Me, *p*-Me, and *m*-H signals of the Mes groups were observed as sharp singlets. Broadening was apparent for the *o*-Me and *p*-Me signals below 0 °C. (See Table II for assignments). The *o*-Me signal splits into three singlets at −14 °C. An average value of 103 Hz was taken as the separation of these signals at −75 °C, which afforded a barrier of 12.3 kcal mol^{-1} for the dynamic process. The *p*-Me signal splits into two peaks (coalescence temperature ~−26 °C), which together with a peak separation of 23 Hz at ~−40 °C, affords a barrier of 12.4 kcal mol^{-1}. The *m*-H signal also splits into three singlets at −19 °C. A rotational barrier of 12.4 kcal mol^{-1} was calculated when an average separation of 52 Hz was used for the *m*-H peaks. The $^1J_{P-H}$ coupling constant remained unchanged in the temperature range +41 to −75 °C.

Mes_2BPPh_2 (2). The ^{1}H NMR spectrum of **2** at various selected temperatures is shown in Figure 8. The *o*-Me, *p*-Me, and *m*-H signals were sharp singlets at room temperature and remained so until fairly low temperatures. A broadening in all signals was noticeable at $T < -65$ °C. The *o*-Me signal was observed to split into two peaks at ~−72 °C, which together with a peak separation of 10 Hz at −98 °C gives a maximum value of 10.1 kcal mol^{-1} for the dynamic process.

$Mes_2BP(t\text{-}Bu)_2$ (3). The ^{1}H NMR spectrum of **3** displayed little evidence of dynamic behavior in the temperature range −97 to +30 °C although a slight broadening was observed at $T < -80$ °C. A maximum value of 8.7 kcal mol^{-1} for a possible dynamic process was estimated by using a T_c of −97 °C, combined with the assumption of a $\Delta\nu$ minimum equal to the width at half-height of the broadest singlet (*o*-Me, 24.0 ± 1 Hz).

$Mes_2BP(1\text{-}Ad)Li(Et_2O)$ (5). The ^{1}H NMR spectrum of **5** at $T < 110$ °C features two signals for the *o*-Me, *p*-Me, and *m*-H groups of the boron mesityls. Only the *p*-Me signals coalesced (at 138 °C) in the temperature range investigated (24–152 °C). The separation between the *p*-Me peaks at 102 °C is 5.4 Hz, which together with the T_c = 138 °C gives a barrier 22.3 kcal mol^{-1} for the dynamic process. The two *o*-Me signals were separated by 54 Hz at 24 °C; this decreased as the temperature was raised, to 28 Hz at 152 °C. A minimum energy barrier of 21.1 kcal mol^{-1} was calculated by assuming $T_c > 152$ °C for the *o*-Me groups. The *m*-H peaks were 15.0 Hz apart at 24 °C, and their separation decreased as the temperature was raised to give a value of 9.6 Hz at 152 °C. A lower limit for the barrier of 22.2 kcal mol^{-1} was obtained in this case.

(22) Kost, D.; Carlson, E. H.; Raban, M. *J. Chem. Soc., Chem. Commun.* **1971**, 656.

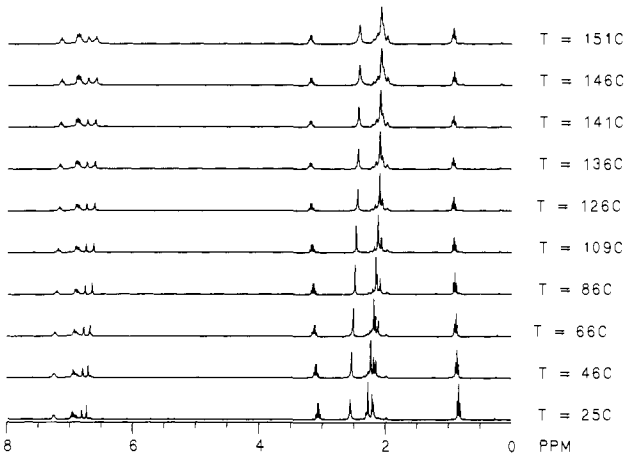

Figure 9. Stacked plot of the variable-temperature ^1H NMR spectra of **6** in a 1:1 mixture of $C_7D_8/o\text{-}C_8C_{10}$.

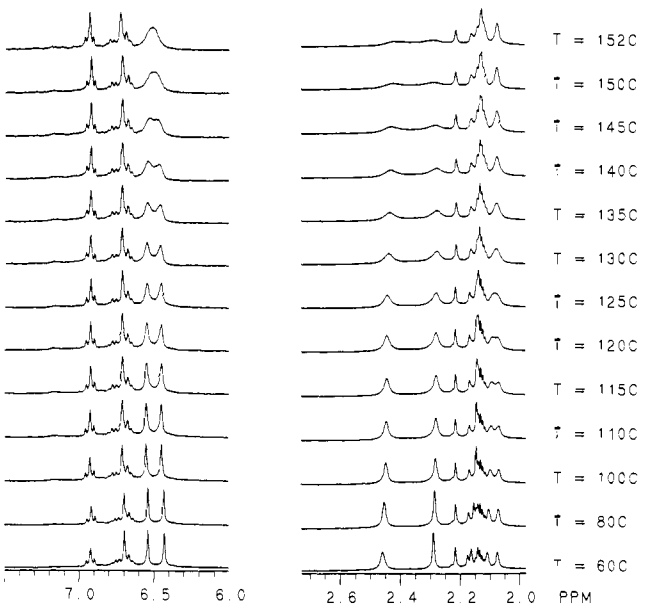

Figure 10. Stacked plot of the variable-temperature ^1H NMR spectra of **7** in $o\text{-}C_8D_{10}$. Signals at 2.14 and at ~2.16 and ~2.22 ppm correspond, respectively, to $o\text{-}C_8D_{10}$ and $(Mes_2B)_2O$.

$Mes_2BP(Ph)Li(Et_2O)$ (6). The VT ^1H NMR spectrum of **6** is illustrated in Figure 9. As in the case of **5**, the *o*-Me, *p*-Me, and *m*-H signals were all observed as pairs of sharp singlets. The downfield *p*-Me signal was merged with the higher field *o*-Me signal at $T > 100$ °C. Only the *p*-Me signals coalesced (at 151 °C) in the range of temperature studied (26–154 °C). The barrier for the dynamic process was calculated to be 22.2 kcal mol^{-1}.

$(Mes_2B)_2PPh$ (7). The VT ^{1}HNMR spectrum of **7** is illustrated in Figure 10. The spectrum at $T < 100$ °C displayed pairs of signals for the *o*-Me, *p*-Me, and *m*-H groups of the mesityl rings. The coalescence temperatures for the *p*-Me and *m*-H signals were at 130 and 150 °C, respectively; the *o*-Me groups were not seen to coalesce up to 155 °C. The maximum separations for the *p*-Me and *m*-H signals were 12.3 and 34.6 Hz. The corresponding values for the dynamic process were calculated to be 21.2 nd 21.4 kcal mol^{-1}.

$Mes_2BP(1\text{-}Ad)PPh_2$ (8). The ^1H NMR spectrum of **8** in the range -99 °C $< T < +70$ °C featured pairs of signals for the *m*-H and *p*-Me groups of the mesityl substituents. The *o*-Me signal was partially obscured by that of the bridgehead adamantyl hydrogens at room temperature. For the *p*-Me and *o*-Me signals, the coalescence temperatures were 120 and 156 °C, respectively. The maximum separation for each pair of signals (7 Hz, *p*-Me; 51 Hz, *o*-Me) occurred near 27 °C. The energy barriers were calculated to be 21.1 (*p*-Me) and 21.4 kcal mol^{-1} (*o*-Me).

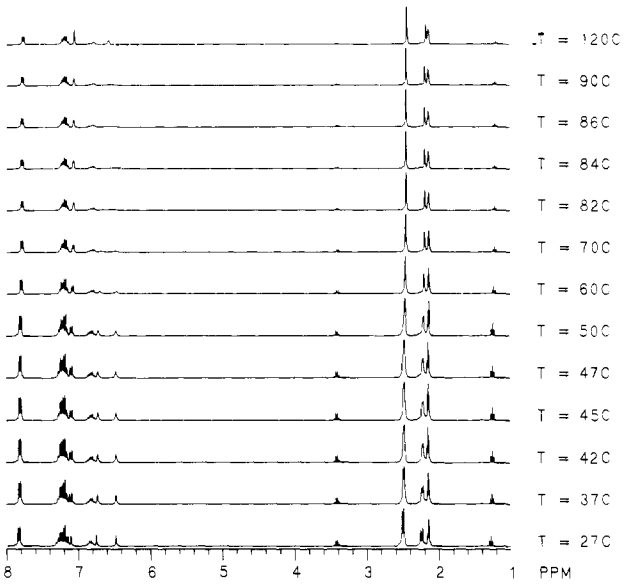

Figure 11. Stacked plot of the variable-temperature ^1H NMR spectra of **9** in $o\text{-}C_8D_{10}$.

$Mes_2BP(Ph)SiPh_3$ (9). The VT ^1H NMR spectrum of **9** is illustrated in Figure 11. The behavior is similar to that described for **5–8** in that the *o*-Me, *p*-Me, and *m*-H signals were pairs of sharp singlets at room temperature. These coalesced at 47 (*o*-Me), 86 (*m*-H) and 50 °C (*p*-Me), respectively. The separation values were 7, 86, and 10 Hz. The calculated energy barriers had the consistent values 17.0 (*o*-Me), 17.4 (*m*-H), and 17.0 (*p*-Me) kcal mol^{-1}.

$Mes_2BP(1\text{-}Ad)SiMe_3$ (10). The ^1H NMR spectrum of **10** at 19 °C features pairs of sharp singlets for the *o*-Me group and *m*-H's, whereas the *p*-Me signal appeared as a singlet. As the temperature was increased, the *o*-Me signals coalesced at 43 °C, affording a value of 16.9 kcal mol^{-1} for the energy barrier when the separation at −25 °C, 5.7 Hz, was used in the calculations. The *m*-H's remained magnetically inequivalent at temperatures as high as 150 °C. The *p*-Me signal unexpectedly splits at 90 °C; the separation between the singlets increased with temperature from 3.0 Hz at 110 °C to 5.4 Hz at 150 °C. The splitting is reversible upon cooling, and this phenomenon is reproducible in both C_7D_8 and C_8D_{10} solvents. As the temeprature was brought below 0 °C, the *p*-Me signal split into two singlets separated by 3.9 Hz at −15 °C. The corresponding temperature of coalescence is 2 °C, which gives a value of 14.9 kcal mol^{-1} for the energy barrier. Further cooling produced a noticeable broadening and decrease in height of the *o*-Me and *m*-hydrogen pair of singlets with respect to the signals of the *p*-Me and $SiMe_3$ groups. Coalescence into broad signals was observed at −74 °C (*o*-Me) and at −89 °C (*m*-H). However, by $T = -99$ °C, these broad signals were not yet split into sets of three singlets. Maximum values of 9.65 (*o*-Me) and 9.26 (*m*-H) kcal mol^{-1} were extrapolated for the inversion barrier at phosphorus by assuming the minimum $\Delta\nu$s as equal to half of the $\nu_{1/2}$ of the broad signals at −99 °C and 47.5 and 17.1 Hz, respectively.

Discussion

Syntheses. A common feature of the compounds in this paper is the use of crowding substituents at boron (usually two mesityl groups) to prevent the association normally observed in B–P compounds. Theoretically, it is possible to achieve the same result by using bulky groups at phosphorus, but since boron is the smaller of the two atoms (radii 0.85 vs 1.11 Å),[23] it is more easily protected. Crowding the boron atom has the further advanage of permitting the use of small groups at phosphorus while retaining

(23) Covalent radii estimated from homonuclear bond lengths: Sutton, L., Ed. Tables of Interatomic Distances and Configurations in Molecules and Ions. *Spec. Publ.-Chem. Soc.* **1958**, *11*; *Spec. Publ.-Chem. Soc.* **1965**, *18*. Slater, J. C. *J. Chem. Phys.* **1964**, *41*, 3199.

monomeric character. This allows the variation in geometry, with substituent size, at the phosphorus center to be studied. The syntheses of compounds **1–10** involve, as the first step, the lithiation of a primary or secondary phosphane with *n*-BuLi, followed by a salt-elimination reaction with Mes_2BF at 0 °C as shown. However, when the second step is carried out at room temperature, the product generally obtained is not the desired phosphinoborane (eq 1). Instead, the dimesitylborane[24,25] is obtained when R′ =

$$RR'PH + n\text{-BuLi} \xrightarrow[Et_2O]{} RR'PLi \xrightarrow[Et_2O]{Mes_2BF} RR'PBMes_2 + LiF\downarrow \quad (1)$$

R′ = H, alkyl, aryl

H (eq 2) whereas the bis(dimesitylboryl) oxide[26] results when R′ = alkyl or aryl (eq 3). Isolation of products having B–O and B–H bonds from reactions 2 and 3 is reproducible. Since the utmost care was taken to exclude moisture and oxygen at all times, it is probable that the unexpected products arise from attack on the solvent ether. Equation 3 is also favored when R and R′ are very bulky. Thus, compounds **3**, **4**, and **7** were obtained as mixtures

$$RP(H)Li + Mes_2BF \xrightarrow{Et_2O} LiF\downarrow + \tfrac{1}{2}(Mes_2BH)_2 + RPH_2 \quad (2)$$

$$RR'PLi + Mes_2BF \xrightarrow{Et_2O} LiF\downarrow + \tfrac{1}{2}(Mes_2B)_2O + RR'PH \quad (3)$$

of the desired product and the diboryl oxide. In the case of **3** or **4**, separation can be easily effected by recrystallization from cold ether, since the diboryl oxide is markedly less soluble than **3** and **4**. In the solid state, it may be easily separated as white needles from the blocklike yellow crystals of **3** and **4**. Compound **7**, on the other hand, has solubility in ether, hexane, pentane, toluene, and benzene very similar to that of the diboryl oxide and could not be obtained without some of this (<10%, monitored by ^1H or ^{11}B NMR spectroscopy) as contaminant. Compounds **1–10** are air- and water-sensitive. In the absence of air, they react with water to give Mes_2BOH[27,28] and the corresponding phosphine.

Structures. In the series of compounds listed in Table I, **2** represented the first structural characterization of a monomeric borylphosphane that had only simple hydrocarbyl substituents.[16] This allowed an assessment of the B–P π-dative interaction in the absence of competing ligands on boron. Shortly before that paper, the structure of the monomeric phosphinoborylamine species tmp(Cl)BP(H)Mes, **13** (tmp = 2,2,6,6-tetramethylpiperidine), was published.[29] In this molecule, the planar boron and nitrogen centers interact strongly (B–N = 1.380 (3) Å), which greatly reduces any multiple B–P bonding. This is reflected in a large (~90°) twist angle between the phosphorus lone pair and the boron p-orbital. Moreover, the P coordination is strongly pyramidal ($\sum°P$ = 307.1°), and the B–P distance is 1.948 (3) Å, consistent with a B–P single bond. In contrast, all the B–P bonds in Table I are shorter than this value and span the range 1.810 (4) to 1.927 (3) Å. Oddly, both of these extremes of B–P distances are found in the unique species **11**.[30] The majority of the compounds have B–P bond lengths in the range 1.82–1.9 Å, and **2**, which has a B–P bond of 1.859 (3) Å, falls almost exactly in the middle of this range. The less hindered compound **1** has a longer bond of almost 1.9 Å, whereas the more crowded species **3** and **4** have B–P bonds of about 1.84 Å. The shortening observed in the B–P bonds of Table I arises from two sources: (i) the formation of a B–P π bond and (ii) the rehybridization at phosphorus. The radius of sp^2-hybridized (i.e., planar) phosphorus is 1.05 Å.[18] When added to the boron radius of 0.85 Å, a B–P bond length of 1.9 Å is predicted. It may be inferred that, in compounds involving planar B and P centers, bond lengths shorter than this value involve a B–P π component.

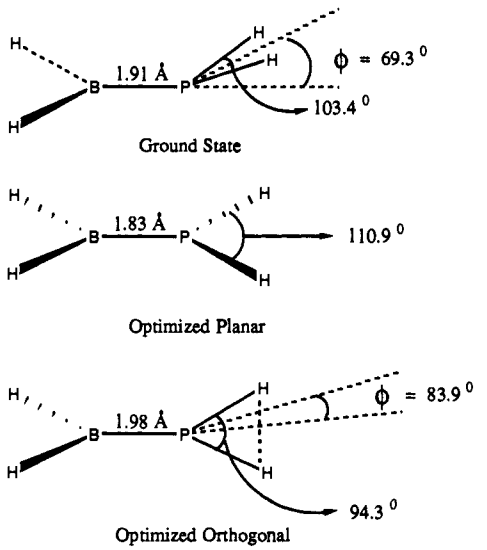

Figure 12. Schematic illustration of the calculated geometries of three configurations of H_2BPH_2.[9]

Compounds **1–4** may be considered as organic derivatives of the parent borylphosphane, H_2BPH_2. The structural data for **1–4** clearly show that the geometry at phosphorus and the B–P bond length are dependent on the size of the phosphorus substituents. In the absence of crowding groups at phosphorus, it is evident that the pyramidal geometry at the P center and a weaker B–P bond are preferred over the planar configuration. This result is in agreement with theoretical work.[9–11] The earliest such calculations on the H_2BPH_2 ground state predicted a pyramidal geometry at phosphorus and a B–P bond of 1.91 Å.[9] The calculated geometries of some configurations of this molecule are illustrated in Figure 12. This prediction is in good agreement with the experimental data for **1**. The most recent theoretical studies (see below), which use more sophisticated mathematical models, also describe H_2B-PH_2 to be nonplanar, with a 70° out of plane angle at phosphorus and a B–P bond of 1.901 Å. On going from the nonplanar to the planar configuration, the B–P bond length decreases from 1.901 to 1.807 Å. A similar trend is apparent in the compounds **1–4**. The bond lengths in this series vary from 1.897 (3) to 1.839 (8) Å, and the data for **1** agree with the lowest energy configuration for H_2BPH_2. The B–P distance of 1.839 (8) Å, found in the almost planar structure of **4**, is longer than the theoretical value of 1.807 Å. This lengthening may be due to the higher steric requirements of the organic substituents.

On the basis of the theoretical data, it has been argued that there is an approximately linear dependence of the B–P bond length on the out of plane angle at P.[11] This approach predicts a value of 1.864 Å for the B–P distance in **2**, which is in good agreement with its experimental bond length of 1.859 (3) Å. As already mentioned, however, the agreement is not so close in the case of **3** and **4** and the longer than predicted B–P distance may be a result of the greater crowding in these molecules. A closer inspection of the two crystallographic independent molecules of **3** reveals some interesting points. It is clear that, in these molecules, the sum of the angles at P implies almost planar configurations at phosphorus. Nonetheless, it can be seen from the data in Table I that the shorter B–P distance corresponds to the larger out of plane angle ϕ. This anomaly may be explained by the differences in the twist angle, the smaller angle being associated with the shorter bond. Clearly, in any consideration of the bonding in these compounds, the twist angle between the phosphorus lone pair and the boron p-orbital also plays an important role.

(24) Hooz, J.; Akiyama, S.; Cedar, F. J.; Bennett, M. J.; Tuggle, R. M. *J. Am. Chem. Soc.* **1974**, *96*, 274.
(25) Bartlett, R. A.; Dias, H. V. R.; Olmstead, M. M.; Power, P. P.; Weese, K. J. *Organometallics* **1990**, *9*, 146.
(26) Cardin, C. J.; Parge, H.; Wilson, J. *J. Chem. Res., Miniprint* **1983**, 810.
(27) Brown, H. C.; Dodson, V. H. *J. Am. Chem. Soc.* **1957**, *79*, 2302.
(28) Weese, K. J.; Bartlett, R. A.; Murray, B. D.; Olmstead, M. M.; Power, P. P. *Inorg. Chem.* **1987**, *26*, 2409.
(29) Arif, A. M.; Cowley, A. H.; Pakulski, M.; Power, J. M. *J. Chem. Soc., Chem. Commun.* **1986**, 889.

The structure of **5** enabled the first direct comparison between a borylphosphine precursor (in this case **1**) and its lithium salt. Although the structures of some borylphosphide salts like **5** had already been reported,[30,31] data for the precursor borylphophine had not been available previously. Only in the case of the unique compound **11**, which has the groups P(H)Mes and P{Li-$(Et_2O)_2$}Mes attached to a common boron center,[30] could a comparison of this kind be made. The facile removal of the H substituent by **1** in *n*-BuLi leads to a change in the coordination at phosphorus from pyramidal to almost planar and a considerable strengthening of the B-P bond. The replacement of H by the $Li(Et_2O)_2$ moiety is accompanied by a change in the B-P distance from 1.897 (3) to 1.823 (8) Å. This is in spite of an increase in the twist angle from 7.5° in **1** to 13.8° in **5**. The corresponding change in **11** is even more dramatic—from 1.927 (3) Å to 1.810 (4) Å. The larger difference seen in the case of **11** is open to a number of interpretations. For example, it could be argued that the B-P distance in **5** is longer than that in **11** because the B center is more crowded owing to the presence of two mesityl substituents. The phosphorus atom, which is bound to adamantyl, $Li(Et_2O)_2$, and $-BMes_2$ groups, is also crowded. The larger twist angle between the B and P planes in **5** seems to bear out this argument. In contrast, the B center in the precursor to **11**—TripB-$(PHMes)_2$—is not as crowded because of the two relatively long bonds to two second-row substituents. Replacement of one H by lithium results in the planarization of the corresponding P center and concomitant shortening in the B-P bond. A very low twist angle and shorter B-P bond is permitted by the lower crowding at B. The dominance of the multiple bonding by one P center seems to exclude interaction with the other so that a large difference in B-P bonds results.

The silyl-substituted compounds **9** and **10** were synthesized to investigate the effect of the electronegativity of the P substituents on B-P bonding. They are the first silyl-substituted phosphinoboranes to be structurally characterized. Prior to discussing their structures, it is worthwhile to refer to the bonding in the silyl-substituted lithium borylphosphide **12**. Its major structural features[30] are similar to those observed for **5** and its analogues.[30,31] The B-P distance 1.833 (6) Å is marginally longer than that observed in **5**. This may, in part, be a result of the solvation of Li by three THFs. The resultant higher steric crowding may induce the rather large twist angle 23.15°, which would result in a longer B-P bond. The structures of **9** and **10** resemble those of **2**-**4** most closely. In fact, **2** and **9** only differ in the fact that one of the phenyl groups is replaced by the more electropositive $-SiPh_3$ substituent. This change leads to an almost planar P center and a B-P bond with enhanced multiple character. It is possible to account for this structural change by assuming the flattening at the phosphorus center is due solely to the increased electron density on phosphorus that arises from the poor electron-withdrawing power of Si relative to C. This rationale is based on an analogy with the lower inversion barriers that have been observed in phosphanes when alkyl or aryl groups are replaced by silyl substituents.[32] The tendency toward flatter P centers in **1**-**4** as the bulkiness of its substituents increases cannot be ignored, however. Thus, the change of coordination at phosphorus in **9** might be due to the larger steric requirements of the triphenylsilyl substituent. However, there are arguments against this explanation. First, the twist angle in **9** is considerably less than those in **3**, suggesting that the crowding in **9** is not severe. In addition, the longer P-Si bond relative to P-C ensures less crowding at the phosphorus center.

The P-Si bond length of 2.231 (3) Å in **9** agrees well with the value predicted by the covalent radii for three-coordinate P (1.05 Å)[18] and tetrahedral Si (1.18 Å).[23] The average C-Si distance of 1.875 (8) Å is also normal for Si bound to sp^2-hybridized carbons. Remarkably, the P-Si bond in **10** is over 0.2 Å longer (2.464 (3) Å), whereas the average C-Si bond length of 1.856 (7) Å is rather short for the sp^3-hybridized carbon atoms involved. The latter distortions may be attributed to the large combined steric requirements of the 1-Ad, $-SiMe_3$, and Mes_2B groups. In essence, the P-Si bonds in **9**, and especially in **10**, are significantly longer than the corresponding one in **12**, 2.213 (2) Å. One explanation of the shortening could involve the more polar character of the phosphorus center in the latter species. This argument is, however, difficult to sustain since in the reported structures $[\{Li(THF)_2P(SiMe_3)_2\}_2]$ and $[Li_4\{\mu_2\text{-}P(SiMe_3)_2\}\{\mu_3\text{-}P(SiMe_3)_2\}_2(THF)_2]$[33] the P-Si bonds are 2.195 (5) and 2.21 Å (av) long. Furthermore, in these lithium salts the P centers are four-coordinate. The discrepancy between these values and those observed in **9**, **10**, and **12** is quite remarkable and indicates significantly weakened P-Si bonds. This is most true in the case of **10**, and the weakened nature of the P-Si bond in this molecule may be responsible for some unusual features of its VT ^1H NMR spectrum (see below).

^{11}B and ^{31}P NMR Studies. Boron-phosphorus compounds with organic substituents readily lend themselves to study by NMR spectroscopy because of the variety of nuclei—^1H, ^{13}C, ^{11}B, ^{31}P—that are amenable to observation. Those most intimately connected with the B-P bonding are, of course, the ^{11}B and ^{31}P nuclei. Unfortunately, asymmetric environments at the B centers result in broad peaks. Consequently, coupling between B and P, which should be an accurate probe of the hybridization at P, is not generally resolved. Table II provides a listing of ^{11}B, ^{31}P, and ^1H NMR data for compounds **1**-**10**. The ^{31}P data for **1**, δ = 0.45 ppm and ^1J(P-H) = 275 Hz, fall within the ranges observed for other secondary borylphosphanes (−2 to −66 ppm, 255-301 Hz).[30] The good agreement of these data confirms that the previously reported compounds $Mes_2BP(R)H$, with R = *t*-Bu, Mes, c-C_6H_{11}, or Ph, are monomeric in the solid state and have three-coordinate B and P centers linked by a bond with some multiple character. The P-H coupling constants of **1** and its analogues are large in comparison to the observed range of 180-230 Hz in normal secondary phosphanes.[34] This has been accounted for in terms of an increase in the s-character of the σ bonds as a result of the wider angles at P.[30] The higher ν_{P-H} stretching frequencies observed for **1** (2330 and 2285 cm^{-1}) in comparison to that in 1-$AdPH_2$ (2275 cm^{-1}) also support this argument. The ^{11}B signal for **1**, a broad peak at 83.8 ppm, is indicative of a three-coordinate environment at B. The ^{11}B shifts observed for **2**, **3**, and **4** are also in the range for three coordination.[35] More variation is found in the ^{31}P chemical shifts and the low δ values, which may be accounted for in terms of the drift of electron density from phosphorus into the boron p-orbital. Even the +I effect of the boron substituent is apparently insufficient to offset these substantial downfield shifts.

The ^{31}P NMR chemical shifts of **5** and **6** were observed 90 and 76 ppm downfield of the precursors **1** and $Mes_2BP(Ph)H$.[30] The deshielding of the phosphorus centers can be explained in terms of a more effective removal of electron density from the planar sp^2-hybridized P center into the B p-orbital. Another factor that contributes to the downfield shifts is the weak association to the Li^+ ion. It has been shown that the Li^+ ion can be easily removed by 12-crown-4.[30,31] Thus, the P centers in **5** and **6** may be regarded as incipiently two-coordinated, which contributes to the observed downfield shifts. In contrast, an upfield shift is observed for the ^{31}P signals of compounds **9** and **10**. Presumably, the replacement of one of the hydrocarbyl groups by a more electropositive silyl substituent leads to a higher electron density on the phosphorus atom, and a shielding effect is observed. The reported ^{31}P chemical shift of $Mes_2BP(SiMe_3)Li(THF)_3$, **12**, is also upfield in comparison

(30) Bartlett, R. A.; Dias, H. V. R.; Feng, X.; Power, P. P. *J. Am. Chem. Soc.* **1989**, *111*, 1306.
(31) Bartlett, R. A.; Feng, X.; Power, P. P. *J. Am. Chem. Soc.* **1986**, *108*, 6817.
(32) (a) Baechler, R. D.; Mislow, K. *J. Am. Chem. Soc.* **1970**, *92*, 4758; (b) *J. Am. Chem. Soc.* **1971**, *93*, 773.
(33) Hey, E.; Hitchcock, P. B.; Lappert, M. F.; Rai, A. K. *J. Organomet. Chem.* **1987**, *325*, 1.
(34) Mark, V.; Dungan, C. H.; Crutchfield, M. M.; van Wazer, J. R. In *Topics in Phosphorus Chemistry*, Grayson, M., Griffith, E. J., Eds.; Wiley: New York, 1967; Vol. 5, Chapter 4.
(35) Nöth, H.; Wrackmeyer, B. *Nuclear Magnetic Resonance Spectroscopy of Boron Compounds*; Springer Verlag: Berlin, 1978.

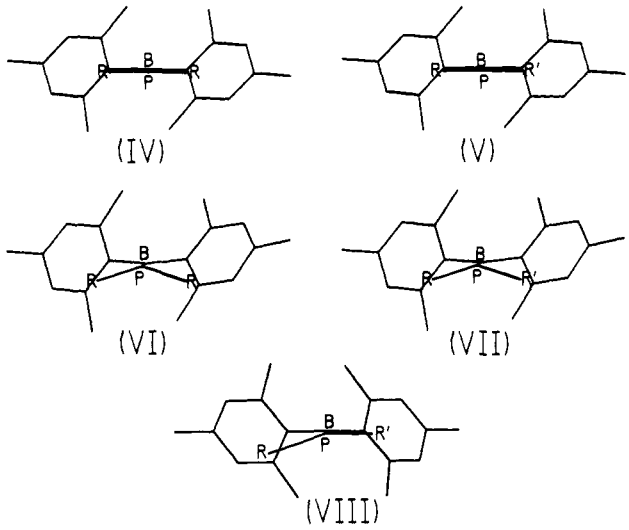

Figure 13. Schematic drawings of five possible configurations of $Mes_2BP(R)R'$ in solution.

to those of the hydrocarbyl-substituted lithium borylphosphides.[30]

The ^{11}B NMR spectra of **1–10** all exhibit broad signals ($\nu_{1/2}$ = 413–1600 Hz) in the range of 85–45 ppm, as expected for three-coordinate B centers.[35] The ^{11}B chemical shifts of phosphinoboranes are less responsive than the ^{31}P NMR shifts to changes in the B–P multiple character, as illustrated by the essentially identical values observed for **1** and **5**. The ^{11}B–^{31}P coupling constants could not be measured in either the ^{11}B or the ^{31}P NMR spectra of compounds **1–10**. Cooling of the samples did not help the resolution of the signals.

Variable-Temperature ^1H NMR Studies. Dynamic ^1H NMR data is provided in Table III. These data represent the first such studies for phosphinoborane and related species that have B–P bonds with multiple character. The most relevant prior VT NMR work has concerned the ring species as illustrated.

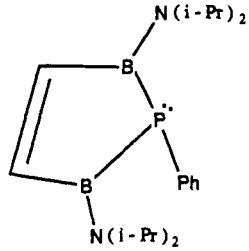

The inversion barrier at phosphorus in the five-membered ring phosphadiborole derivative has been estimated[36] at 10–15 kcal mol^{-1}. However, the coplanarity of the boron and nitrogen planes in this compound together with the B–P distance of 1.949 (2) Å and the sum of the angles at P of 259.9° suggests that the π-interaction between the boron and phosphorus in this compound is low.

Dynamic Processes in Compounds 1–10. The variable-temperature ^1H NMR studies in this paper are, for the most part, contingent upon the detection of magnetic inequivalance in the mesityl groups of a $-BMes_2$ moiety attached to a phosphorus center. This may be readily appreciated by inspection of the schematic drawings in Figure 13. Several different conformational changes may occur that may, in theory at least, be observed by ^1H NMR. The major ones involve inversion at the P center, rotation about the B–P bond, and rotation around the B–C bonds.

In the very simplest case (IV), where there are equivalent substituents on P and a planar or near planar geometry at P, no dynamic behavior should be observed unless the Mes planes are frozen in an angular orientation with respect to the boron plane.[37] Compounds **3** and **4** fall into category IV, and they display no splitting of the Mes signals at temperatures as low as −97 °C. This observation implies that stereoisomerization as a result of flipping of the Mes groups remains rapid at low temperature or that the mesityl planes are "frozen" in positions that are approximately perpendicular to the boron plane. The observation of barriers as high as 12 kcal mol^{-1} for mesityl ring flip in Mes_2BOMe[37] suggests that the latter possibility is the more likely in the case of **3** and **4**. On the basis of the existing structural similarities between compounds **3**, **4**, and **9**, **10**, discussed earlier, it is highly probable that the rotation barriers for the B–P bonds of **3** and **4** are similar to those of **9** and **10**. This implies that the rotation around the B–P bonds of **3** and **4** is slow (but not observable) on the NMR time scale at temperatures below about 0 °C. In V, however, which has an approximately planar C_2B–PCC′ framework, two sets of boron mesityl peaks should be observed when the rotation around the B–P bond is slow owing to the different magnetic environments created by the inequivalent substituents on phosphorus. Moreover, the observation of inequivalence in the mesityl signals should not be dependent on restricted rotation around the B–C bond. This bonding model is expected to correspond approximately to the dynamic behavior of **5–10**, owing to the planarity of the phosphorus geometry in their X-ray structures. These compounds are characterized by substantial B–P rotational barriers of 16–22.3 kcal mol^{-1}.

Other configurations for the B–P system are also possible. Two related cases are illustrated by VI and VII. In these, the P center has pyramidal geometry. In the case of VI, the P substituents are identical, whereas in VII, they are different. When the molecule is in the conformation depicted by VI, inequivalent *o*-Me signals may be observed in a 1:1 ratio provided that rotation around the B–C bond is slow. In VII, however, a slightly more complex spectrum should be obtained owing to the differential substitution at phosphorus. In this case, provided B–C rotation (Mes ring flip) is absent, three *o*-Me signals in a 2:1:1 ratio should be obtained. If there is rapid B–C rotation, two *o*-Me signals should be seen. The VT ^1H NMR spectra of **1** (Figure 7) and **2** (Figure 8) correspond to these two models. It is, of course, possible to explain the dynamic behavior of **2** on the basis of slow Mes ring flipping and continued rapid inversion at P. This explanation, however, is not supported by the spectrum of **1**, which has a 2:1:1 intensity ratio of the *o*-Me groups. Thus, it appears that the dynamic process observed in **2** is a result of inversion at phosphorus, which has a maximum ΔG value of ~10 kcal mol^{-1}.

A major problem in the interpretation of the ^1H NMR data is that it may not always be possible to uncouple the processes of inversion and rotation in the B–P moiety. The subtleties of this question may be illustrated in the VT ^1H NMR behavior of **1** (Figure 7). At −75 °C, the inversion at P and the rotations around the B–P and the B–C bonds are apparently slow on the NMR time scale. At this temperature, three signals are observed for both the *o*-Me and *m*-H groups in accordance with model VII, whereas only two signals are observed for the *p*-Me groups. As the temperature is raised, the *p*-Me pair of singlets were observed to coalesce into one peak. This is to be expected only when there is rapid rotation around the B–P bond because simple inversion at P or rapid rotation around the B–C bonds should not result in the coalescence of the two *p*-Me signals. The two groups of three signals of the *p*-Me and the *m*-H each coalesce directly into one signal without first becoming pairs of singlets. The latter behavior is expected if the inversion energy barrier is higher than the rotational one. Thus, the value of 12.4 kcal mol^{-1} corresponds to the rotational energy barrier around the B–P multiple bond in **1**. The invariance of the $^1J_{P-H}$ value over the −65 to +41 °C temperature range also supports this view. An upper limit of 12.4 kcal mol^{-1} for the inversion barrier is implied by the spectral data in Figure 7.

At least one other conformation (VIII) for phosphinoboranes is possible. In VIII, the P center is nonplanar and there are two

(36) Driess, M.; Pritzkow, H.; Siebert, W. *Angew. Chem.* **1987**, *99*, 789; *Angew. Chem., Int. Ed. Engl.* **1987**, *26*, 781.

(37) Finocchiaro, P.; Gust, D.; Mislow, K. *J. Am. Chem. Soc.* **1973**, *95*, 7029.

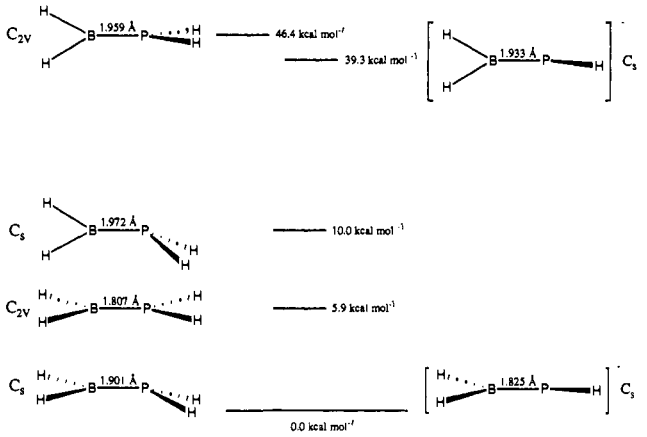

Figure 14. Calculated structural and energy data for various configurations of H_2BPH_2 and H_2BPH^-.[11]

different substituents at P. One P–R vector is almost exactly aligned with the B–C_2 plane whereas the other P–R′ (often from a weakly bound R′ group) vector has a considerable out of plane angle. Compound **10** may fall into this category.

Inversion and Rotation Barriers in 1–10. The data in Table III may be compared with theoretical values calculated for the parent phophinoborane H_2BPH_2, and the anion H_2BPH^-. The calculated structural and energy data for different configurations[11] of these two species are given in Figure 14. For H_2BPH_2, the ground state is calculated to have the pyramidal geometry of phosphorus as illustrated previously in Figure 12. If the energy of this is set at zero, the planar (C_{2v}) form is calculated to be 5.9 kcal mol^{-1} less stable whereas the two twist configurations have energies 10.0 and 46.4 kcal mol^{-1} above the ground state. The data thus indicate that the inversion barrier at phosphorus is 5 kcal mol^{-1} and the rotation barrier may vary over the range 10.0–46.4 kcal mol^{-1}. These values may be compared with previous estimates[9,10c] of 8.14 and 4.2 kcal mol^{-1} for the inversion barrier and a range of 6.56–48.5 or 10.6–44.2 kcal mol^{-1} for the rotation barrier. The rotational barrier for H_2BPH^-, which has a planar ground state, is calculated to be 33.5 kcal mol^{-1}.[11]

The sole unambiguous determination of an inversion barrier in compounds **1–10** concerns **2**, and in this species it is about 9 kcal mol^{-1}. Indirect support for this value comes from data for **1**, **3**, and **10**, which indicate maximum possible inversion barriers of about 12.4, 9, and 9.5 kcal mol^{-1} in these compounds. These values are higher than those predicted by the data in Figure 14. It is notable, however, that they are a great deal less than the inversion barrier for PH_3 (36.7 kcal mol^{-1})[38] and its organic derivatives (32–40 kcal mol^{-1}).[39] It has been established that inversion barriers in phosphanes are greatly affected by inductive effects of the substituent. Thus, silylphosphanes have greatly reduced phosphorus inversion barriers (12–19 kcal mol^{-1})[32] whereas halophosphanes are calculated to have much higher barriers, e.g., 54.1 kcal mol^{-1} in $P(F)Me_2$.[39] No doubt part of the reason for the lower inversion barriers in borylphosphanes is the inductive effect of the boron substituent. Nonetheless, if this parameter were the sole determinant of inversion barrier, the values for phosphinoboranes should be greater than those of silylphosphanes owing to the greater electronegativity of boron (B (2.01) vs Si (1.74)).[40] It is found, however, that the barriers in phosphinoboranes are lower than those in silylphosphanes. The main reason for this is the large stabilization of the planar transition state due to strong conjugation of the phosphorus lone pair with the empty boron p-orbital, i.e., a strong B–P π-interaction.[9–11] Thus, the ground state of phophinoboranes is pyramidal rather than planar, not because the PR_2 moiety is a poor π-donor but because of the great stabilization of the phosphorus lone pair orbital. It energy terms, the planarization of phosphorus is very expensive and it requires a strong π-bond to achieve planarity, even in the presence of bulky or electropositive substituents at phosphorus.

The structural data in Table I show that a planar geometry at phosphorus may be induced by three different methods: (a) bulky substituents as exemplified by **3** and **4**; (b) electropositive substituents as exemplified by **5**, **6**, **11**, and **12**; (c) more extensive delocalization of the phosphorus lone pair, for example, **7**. Recent work[41] (vide infra) has shown that the boron substituent may also exert considerable influence on the B–P bond. A combination of (a) and (b) may account for the planar or near-planar geometries at phosphorus in **8**, **9**, and **10**. The highest rotation barriers (~22 kcal mol^{-1}) were observed for the lithium salts **5** and **6**. Prior structural work[30,31] has shown that the Li^+ ion is weakly associated with the phosphorus center and the B–P bond length is very little changed by removing the Li^+ ion. It seems therefore reasonable to assume that the energy barriers in **5** and **6** would be only slightly affected by removal of the Li^+ ion. The energy barriers in **5** and **6** may be compared with the calculated value (33 kcal mol^{-1}) for the $[H_2BPH]^-$ ion.[11] The large difference between experiment and theory may be due, in part, to the effects of the size of the substituents. Bulky groups are expected to destabilize a ground state in which the boron and phosphorus substituents are eclipsed. Evidence for this destabilization comes from twist angles between the B and P planes—as high as 23° in the case of **12**.[30] Inductive effects involving the replacement of hydrogens by hydrocarbyl groups may also play a role.

High rotational barriers were also observed in the compounds **7** and **8**. The structure of **7** features an extended planar array involving P, the two B centers, and the five ipso carbons. The PB_2 array is thus an isolobal analogue of the allyl cation.[17] Some interesting theoretical data have appeared[42] concerning the model compound for this species, $HP(BH_2)_2$. These data suggest the existence of a synergic substitution effect in which the presence of more than one boryl substituent on phosphorus serves to enhance both B–P π-interactions. The calculated BP rotation barrier in $HP(BH_2)_2$ is 17.5 kcal mol^{-1}. The VT ^{1}H NMR data for **7** show that there is a large rotational barrier (~21 kcal mol^{-1}) in moderately good agreement with the theoretical prediction. Important structural work[41] on the related compounds $EtOB(PMes_2)_2$ and $BrB(PMes_2)_2$ has clearly shown that the boron substituent has a considerable effect on the B–P multiple bonding, which is stronger where there is a more electron withdrawing substituent (Br) on boron. Spectroscopic data on the species Mes-BPPhC$_6$H$_4$PPh[43] have also appeared, but no dynamic ^{1}H NMR studies of either this compound or the species $XB(PMes_2)_2$ (X = Br, OEt) have been reported. The high barrier in **8** is difficult to explain on the basis of steric and inductive effects in the ground state alone. It may be that the excited state (Figure 14) is destabilized by the presence of the $-PPh_2$ and 1-Ad groups on phosphorus. These two substituents may permit little steric flexibility at the phosphorus so that a rigid, almost planar, geometry close to that of the ground state has to be maintained throughout the rotation process.

For the compounds **9** and **10**, slightly lower rotation barriers (~17 kcal mol^{-1}) were observed. This finding is in agreement with the fact that the B–P bonds found in **9** and **10** are longer than those in **5** and **6**. The geometry at phosphorus in **9** is close to planar whereas in **10** it is noticeably pyramidal. Inductive effects owing to the presence of the silyl substituents are expected to play a significant role in the determination of the rotational barrier. More electropositive groups are believed to stabilize the planar hybridization at phosphorus in the structures in Figure 14.[32,39] Silyl groups, although electron releasing, are not as effective as Li^+ in this respect. Thus, a simple rationale for the lower

(38) Lehn, J. M.; Munsch, B. *Mol. Phys.* **1972**, *23*, 91.
(39) Rauk, A.; Andose, J. D.; Frick, W. G.; Tang, R.; Mislow, K. *J. Am. Chem. Soc.* **1971**, *93*, 6507.
(40) Allred, A. L.; Rochow, E. G. *J. Inorg. Nucl. Chem.* **1958**, *5*, 264.
(41) Karsch, H. H.; Hanika, G.; Huber, B.; Meindl, K.; König, S.; Kruger, C.; Muller, G. *J. Chem. Soc., Chem. Commun.* **1989**, 373.
(42) Coolidge, M. B.; Borden, W. T. *J. Am. Chem. Soc.* **1990**, *112*, 1704.
(43) Bohra, R.; Hitchcock, P. B.; Lappert, M. F.; Leung, W. P. *J. Chem. Soc., Chem. Commun.* **1989**, 728.

rotation barriers in **9** and **10** has its basis in the less electropositive character of the silyl group in comparison to Li^+.[40] This reduces the electron density on phosphorus in comparison to that in **5** and **6**, which in turn, weakens the P → B π-interaction. The rotation barrier found in **1** is also in harmony with these results. In **1**, it could be argued that the lower barrier results from the different steric effects of the H and the $SiMe_3$ groups. Nonetheless, it should be borne in mind that the crowding ability of $SiMe_3$ is not particularly high owing to the length of the P-Si bond. It is thus more probable that the differences between rotation barriers in **1** and **10** arise from the differences in electronegativity between H and Si.[40]

A feature of the data in Tables I and III is the lack of a strict correlation between the B-P bond lengths and the rotation barriers, or even the pyramidicity, at phosphorus. The main reason for this is that X-ray structural data concerns the ground state only, whereas the rotation process involves both ground and transition states. Thus, **9** and **10**, which have shorter B-P bonds than that in **8**, have lower rotation barriers probably because of different excited-state structures. A further example of a lack of correlation concerns the different B-P distances found in the two $Mes_2BP(t\text{-}Bu)_2$ molecules of **3** where the longer B-P distance is associated with the flatter P center.

The rotation barriers in Table III may also be compared with barriers in similar boron-nitrogen systems such as the aminoboranes.[4,5,44] A major difference between phosphinoboranes and aminoboranes is the much lower inversion barrier at nitrogen in comparison to phosphorus.[39,45] Thus, the formation of a B-N π-bond is much less costly in energy terms than the formation of a B-P π-bond. In addition, the sizes of the B and N atoms suggest that π-overlap would be more efficient for this pair. On this basis, it might be expected that B-N π-bonds would be much stronger than those of B-P. In general, aminoboranes, $R_2BNR'_2$, have rotation barriers in the range 9-24 kcal mol^{-1}.[44] This range of values is, of course, very similar to that found in this study. It may be concluded that B-P π-bonding is at least as strong as B-N π-bonding. This finding is in agreement with the theoretical data on phosphinoboranes[9-11,42] but also with calculations for the B-P analogues of borazines.[46,47] The good π-donor characteristics of the $-PR_2$ group toward boron, implied by these results, are consistent with the lower electronegativity of phosphorus in comparison to nitrogen.[40] In fact, the electronegativities of B and P are very similar.[40] Thus, the B-P pair is not as polar as B-N, which suggests that B-P orbital overlap is quite effective. Also, the relative sizes of the B and P atoms are not as disparate as might be imagined, 0.85 vs 1.11 Å.[23]

In conclusion, the results in this paper demonstrate that although higher inversion barriers at phosphorus (compared to those at nitrogen) may lead to differences in structures in the ground state, B-P π-bonding is quite strong and is comparable to that observed in B-N compounds. It may be anticipated that B-As π-bonding should also be quite substantial, and preliminary results have already indicated that it is almost as high as that seen between boron and phosphorus.[48]

Acknowledgment. We thank the NSF for financial support, Professors T. L. Allen and W. H. Fink for useful discussions and permission to use theoretical data for H_2BPH_2 and $[H_2BPH]^-$, and Dr. M. M. Olmstead for her help in solving the structure of **4**.

Registry No. 1, 130417-24-2; **2**, 105597-78-2; **3**, 136006-13-8; **4**, 136006-14-9; **5**, 136006-15-0; **6**, 118496-22-3; **7**, 116864-37-0; **8**, 131545-45-4; **9**, 136006-16-1; **10**, 136006-17-2; 1-$AdPH_2$, 23906-89-0; Mes_2BF, 436-59-9; Ph_2PH, 829-85-6; $(t\text{-}Bu)_2PH$, 819-19-2; Mes_2PH, 1732-66-7.

Supplementary Material Available: Table summarizing X-ray data collection and refinement, tables of atom coordinates, bond distances and angles, anisotropic thermal parameters, and hydrogen coordinates, and a table with full IR data for **1-3**, **5**, and **10** in the range 4000-200 cm^{-1} (35 pages); tables of observed and calculated structure factors (108 pages). Ordering information is given on any current masthead page.

(44) (a) Barfield, P.; Lappert, M. F.; Lee, J. *Proc. Chem. Soc., London* **1961**, 421; *Trans. Faraday Soc.* **1968**, *64*, 2571. (b) Watanabe, H.; Totini, T.; Tori, K.; Nakagawa, T. *Proc. Colloq. AMPERE* **1965**, *13*, 374. (c) Dewar, M.; Rona, P. *J. Am. Chem. Soc.* **1969**, *91*, 2259. (d) Imbrey, P.; Jaeschke, A.; Friebolin, H. *Org. Magn. Reson.* **1970**, *2*, 271. (e) Neilson, R. H.; Wells, R. L. *Inorg. Chem.* **1977**, *16*, 7.

(45) (a) Andose, J. D.; Lehn, J. M.; Mislow, K.; Wagner, J. *J. Am. Chem. Soc.* **1970**, *92*, 4050. (b) Stackhouse, J.; Baechler, R. D.; Mislow, K. *Tetrahedron Lett.* **1971**, 3437, 3441. (c) Brois, S. J. *Trans. N.Y. Acad. Sci.* **1969**, *31*, 931. (d) Mislow, K. *Trans. N.Y. Acad. Sci.* **1973**, *34*, 227.

(46) Fink, W. H.; Richards, J. *J. Am. Chem. Soc.* **1991**, *113*, 3393.

(47) Power, P. P. *J. Organomet. Chem.* **1990**, *400*, 49.

(48) Dias, H. V. R.; Petrie, M. A.; Shoner, S. C.; Power, P. P. *Angew. Chem., Int. Ed. Engl.* **1990**, *29*, 1033.

Silaamidide Salts: Synthesis, Structure, and Reactions

Gail E. Underiner, Robin P. Tan, Douglas R. Powell, and Robert West*

Contribution from the Department of Chemistry, University of Wisconsin—Madison, Madison, Wisconsin 53706. *Received May 13, 1991*

Abstract: Five silaamidides have been prepared and characterized: lithium *N,N'*-bis(2,4,6-tri-*tert*-butylphenyl)phenylsilaamidide (**2**), lithium *N,N'*-bis(2,4,6-tri-*tert*-butylphenyl)chlorosilaamidide (**5**), lithium *N,N'*-bis(2,4,6-tri-*tert*-butylphenyl)-*n*-butylsilaamidide (**6**), lithium *N,N'*-bis(2,4,6-tri-*tert*-butylphenyl)-*tert*-butylsilaamidide (**7**), and potassium *N,N'*-bis(2,4,6-tri-*tert*-butylphenyl)chlorosilaamidide (**8**). Reactions of silaamidides with alcohols, amines, hydrogen bromide, *n*-butyllithium, and benzaldehyde are described. The structure of **7**·(12-crown-4)(THF) was determined by X-ray analysis: crystals are orthorhombic, space group $Pna2_1$; a = 16.289 (7), b = 17.991 (8), c = 17.965 (8) Å; V = 5265 (4) $Å^3$; d_{calcd} = 1.084 g/mL for Z = 4; R = 5.05%. The Si-N bond distances are 1.594 and 1.626 Å, and the Si and attached N, N, and C atoms are coplanar.

Introduction

The chemistry of multiply bonded silicon has become an active area of research, since the first isolation of such compounds in 1981.[1] Stable compounds are now known with Si=Si,[2] Si=C,[3] Si=N,[4] and Si=P[5] double bonds, and an allylic structure with a silicon atom in the central position, 1,3-diphospha-2-silaallyl

(1) West, R.; Fink, M. J.; Michl, J. *Science (Washington, D. C.)* **1981**, *214*, 1343.

(2) West, R. *Angew. Chem., Int. Ed. Engl.* **1987**, *26*, 1201.

(3) (a) Brook, A. G.; Abdesaken, F.; Gutenkunst, B.; Gutekunst, G.; Kallury, R. K. *J. Chem. Soc., Chem. Commun.* **1981**, *191*. (b) Wiberg, N.; Wagner, G.; Müller, G. *Angew. Chem., Int. Ed. Engl.* **1985**, *24*, 229.

0002-7863/91/1513-8437$02.50/0